Large copepods as leading indicators of walleye pollock recruitment in the southeastern Bering Sea: sample-based and spatio-temporal model (VAST) results

Lisa B. Eisner[a], Ellen M. Yasumiishi[b], Alexander G. Andrews III[b], Cecilia A. O'Leary[a]

[a] NOAA Fisheries, Alaska Fisheries Science Center, 7600 Sand Point Way NE, Seattle, WA, 98115 USA; lisa.eisner@noaa.gov; corresponding author

[b] NOAA Fisheries, Alaska Fisheries Science Center, Auke Bay Labs, 17109 Pt. Lena Loop Rd., Juneau, AK, 99801 USA; ellen.yasumiishi@noaa.gov, alex.andrews@noaa.gov

Abstract

In the southeastern Bering Sea, years with above-average sea ice extent have been associated with elevated abundances of large lipid-rich copepods in both net tows and age-0 walleye pollock (*Gadus chalcogrammus*) diets, followed by high overwinter pollock survival and stronger recruitment into the fishery three years later. In this study, we directly compare large copepod abundances of taxa important in age-0 pollock diets (*Calanus glacialis/marshallae*, *Metridia pacifica* and *Neocalanus* spp.) to age-3 pollock abundance from stock assessments for year classes 2002-2015 (excluding 2013). Copepod samples from bongo nets were collected on fishery oceanography surveys in late summer during warm (low ice) and cold (high ice) climate stanzas. In addition to mean estimates of large copepods among stations (sample-based), we implemented a spatial delta-generalized linear mixed model using the Vector Autoregressive Spatio-Temporal (VAST) package to account for variations in survey coverage among years. Positive significant linear relationships were found for both of these estimates of large copepods during the age-0 year and the abundance of these pollock at age-3. Correlations were stronger using VAST model-based indices compared with sample-based indices (R^2 = 0.74 versus 0.43, respectively, all copepod taxa combined). A significant relationship was also observed between the bottom cold pool (< 2°C) area (indicative of sea ice coverage in the prior winter) during the age-0 year and subsequent age-3 pollock abundance (R^2 = 0.56) and recruits per spawner, (ln(age-3 abundance /spawning stock biomass), R^2 = 0.77). Consequently, the large copepod index or cold pool index may be used to predict future recruitment success of pollock three years in advance. Results provide support for the revised oscillating control hypothesis that suggests as the climate warms, reductions in sea ice and consequent reduced availability of ice-associated

algae, an early spring food source, could be detrimental to large copepods and recruitment of the pollock stock in the region.

Keywords: walleye pollock, *Calanus*, large copepods, Bering Sea, cold pool, VAST

Declarations of interest: none

1. Introduction

Zooplankters are essential agents for the transfer of energy from primary production to fish, seabirds, and marine mammals. In the southeastern Bering Sea, interannual variability in zooplankton abundance has generated considerable interest in how these changes propagate through the food web to higher trophic levels (Coyle et al., 2011; Hunt et al., 2011). Walleye pollock (*Gadus chalcogrammus*, hereafter pollock) is the largest fishery in terms of landed biomass in the eastern Bering Sea with an ex-vessel value of $375 million in 2016 (Fissel et al., 2017). Large lipid-rich crustacean zooplankton, such as large copepods, are important prey during all life stages, and in particular during the larval and juvenile stages of pollock (Andrews et al., 2016; Buckley et al., 2016; Coyle et al., 2011; Strasburger et al., 2014) and thus impact health and growth during critical periods for survival. Notably, the availability of large copepods in late summer may impact energy stores and overwinter survival of age-0 pollock, and subsequent recruitment into the pollock fishery (Heintz et al., 2013; Moss et al., 2009). Commercial fishermen and fisheries managers would benefit from an improved understanding and ability to predict interannual variation in recruitment to help forecast future pollock productivity and consequent fisheries management. Thus, elucidating factors that explain interannual variability in pollock recruitment, such as availability of large copepod prey during the pollock age-0 year, is of critical importance.

The southeastern Bering Sea is characterized by a broad continental shelf (> 500 km wide and > 1000 km long) and supports a highly productive ecosystem due to on-shelf flow of nutrient-rich waters. Persistent oceanographic fronts (Hunt and Stabeno, 2002) separate the shelf into three domains: the inner shelf (< 50 m bathymetry), the middle shelf (50–100 m), and the outer shelf

(100–200 m) (Coachman, 1986; Iverson et al., 1979). During summer, the inner shelf is well mixed, the middle shelf is highly stratified with a wind-mixed surface layer and a tidal-mixed bottom layer, and the outer shelf has a multi-layer system with the surface and bottom layers separated by a gradient (Stabeno et al., 2010). The southeastern Bering Sea shelf is seasonally ice covered during cold climatic periods, and this sea ice leaves a footprint of cold bottom waters < 2ºC (i.e., the cold pool), which extends southward within the middle shelf. The area of the cold pool is determined in large part by where the ice forms, and its temperature depends on the amount of ice that forms above it.

Climate change has led to rapid changes in the southeastern Bering Sea shelf resulting in variations in seasonal sea ice coverage and water column temperatures, which can impact the entire ecosystem (e.g., Napp and Hunt, 2001; Stabeno et al., 2012). In recent years (2001–2016) decadal-scale oscillations (i.e., Aleutian Low Pressure System) have led to climate stanzas with several years of warm ocean temperatures (low ice) followed by several years of cold ocean temperatures (high ice) and again by warm temperatures; this is unlike interannual variations typically observed in prior decades (Stabeno et al., 2012).

Since 2001, the abundance of large copepods has been higher in years with extensive and persistent sea ice (Eisner et al., 2014, 2015; Kimmel et al., 2017). This ice cover results in a more extensive cold pool over the southeastern shelf and in lower bottom temperatures throughout the summer, particularly in the middle shelf region. The presence of sea ice (and ice associated algae) provides an early food source for growth and reproduction for *Calanus marshallae/glacialis* (*Calanus* spp.), the large copepod taxa that contributes most to interannual

86 variations in zooplankton biomass during late summer in the eastern Bering Sea (Baier and
87 Napp, 2003; Eisner et al., 2014). Cooler temperatures during summer and over winter also can
88 enhance survival of *Calanus* spp. (and juvenile pollock) since metabolic rates are lowered and
89 less energy (i.e., less prey) is required for survival in cold water (Coyle et al., 2008; Coyle and
90 Gibson, 2017). In late summer, low bottom temperatures have been associated with increased
91 numbers of large copepods, resulting in increases in the total biomass of large zooplankton
92 (Eisner et al., 2014).
93
94 Prior research has demonstrated that years with relatively high abundances of large lipid-rich
95 copepods in the environment and in juvenile pollock diets (Coyle et al., 2011; Moss et al., 2009)
96 are also years with high energy density (high amounts of storage lipid, kJ per fish) in age-0
97 pollock (Heintz et al., 2013). Age-0 fish with high amounts of lipid are better able to survive
98 their first winter since they are less likely to starve. The high energy density in age-0 pollock has
99 been shown to be positively associated with recruitment of age-3 pollock into the fishery (Heintz
100 et al., 2013).
101
102 Here, we evaluate the relationship between the abundance of large lipid-rich copepods during the
103 summer pollock are age-0 and the abundance of these fish at age-3 to assess the feasibility of
104 predicting recruitment of pollock to the fishery three years in advance. This advanced notice
105 could assist the fishing industry and fisheries managers in governing this important Bering Sea
106 fishery. We also evaluate how climate and associated environmental factors relate to interannual
107 variation in the abundance of these copepods and subsequent abundance of pollock-3 years later.
108 A recently developed spatio-temporal modelling tool, Vector-Autoregressive Spatio-Temporal

(VAST), is explored here to estimate the distribution and abundance of large copepods. VAST was previously used for estimating abundance of fish in the eastern Bering Sea, amongst many other uses (Thorson et al., 2015). We use this method because like other model-based methods, VAST can account for changes in sampling density and spatial extent among years (i.e., spatially unbalanced data) (Thorson et al., 2016b), an issue in our data that is common to field data.

Our four main goals were to 1) develop an estimate from bongo net data of mean late summer abundance and spatial distribution of large copepods important in age-0 pollock diets in the eastern Bering Sea, including *Calanus* spp. (Coyle et al., 2011), *Neocalanus* spp. (Moss et al., 2009; Siddon et al., 2013) and *Metridia pacifica* (Strasburger et al., 2014), 2) evaluate the correlations between these estimates of large copepod abundance and stock assessment indices of age-3 pollock abundance and age-3 pollock abundance per female spawning stock biomass. The latter index, commonly termed recruits per spawner, can be used to avoid confounding maternal and environmental factors and thus may be useful information for stock assessment (Brodziak and O'Brien, 2005; Myers, 2001), 3) determine if correlations can be improved using VAST model-based estimates of copepod abundances over mean estimates of large copepods among stations (sample-based estimates), and 4) evaluate the strength of association between environmental covariates and age-3 pollock indices; to do so, we modeled recruits per spawner using spawning stock biomass, along with copepod and environmental covariates.

2. Methods

We describe the study area and years sampled, data, and statistical analyses performed. Data included abundances of large copepods (sample-based and VAST model-based estimates) and

spawning stock biomass during the age-0 year, and subsequent abundances of age-3 pollock or age-3 pollock/spawning stock biomass (Ianelli et al., 2018). We evaluated environmental variables that reflected variations in temperature and sea ice, climate–related factors that can impact abundances of large copepods and pollock (Eisner et al., 2014; Hunt et al., 2011; Sigler et al., 2016; Stabeno et al., 2012).

2.1 Study area and years sampled

Zooplankton were collected on fishery oceanography surveys conducted by the Bering Arctic Subarctic Integrated Survey (BASIS) field program at the NOAA Alaska Fisheries Science Center (AFSC) during mid-August to late September in the southeastern Bering Sea (Fig. 1). Sample years include seven warm (2002–2005, 2014-2016), one average (2006), and six cold (2007–2012) years. No survey was conducted in 2013, an average year. BASIS stations used in our analysis were spaced 30–60 km apart from 55.0–59.8°N and 160–173°W. The BASIS stations often extended across the outer shelf to the shelf break (~ 180 m bathymetry) south of ~57°N and to the middle shelf front (~ 100 m) bathymetry from 57–60°N. The total sampled survey area considered in our analyses was 3.57016×10^{11} m^2. Data were collected at a total of 901 stations, ranging from 32 stations in 2008 to 87 stations in 2012 (Fig. S.1). Sampling density and spatial extent varied among years. For example, fewer stations covered the same spatial extent creating a lower sampling density (e.g., 2009), the sampling density was the same but the spatial extent was reduced (e.g., 2015), or both sampling density and spatial extent were reduced (e.g., 2008). In contrast to BASIS, the NOAA AFSC summer (June to mid-August) bottom trawl survey, which collects data used in pollock stock assessment estimates, extended to the shelf

break over the entire sampling grid (Fig. 1), and station spacing, 37.04 x 37.04 km (20 x 20 nautical mile) and the area sampled, did not vary among years (Conner and Lauth, 2017).

2.2 Data

2.2.1 Environmental variables

Environmental variables that were likely to impact age-0 pollock survival and subsequent recruitment to age-3 (Heintz et al., 2013; Sigler et al., 2016) initially included sea surface temperature and bottom temperature, the winter ice cover index, and the cold pool index for years 2002–2015. An annual mean sea surface temperature and bottom temperature for the southeastern Bering Sea were calculated from data collected at the same locations each year during the AFSC bottom trawl survey (Fig. 1) (Conner and Lauth, 2017). Station specific temperature and depth data were collected with a Sea-Bird Electronics model 39 datalogger attached to the headrope of the bottom trawl. The ice cover index is an annual index of winter ice coverage in the southeastern Bering Sea; specifically, it is the average ice concentration (10^6 km^2) in a 2° x 2° box (56°–58°N, 163–165°W, Fig. 1) from January 1–March 31. The ice cover index was obtained from the Bering Climate website (https://www.beringclimate.noaa.gov/data/BCresult.php), which is maintained by the NOAA Pacific Marine Environmental Laboratory (PMEL). Data were accessed March 26, 2018 (last updated August 21, 2016). A summer cold pool index for the eastern Bering Sea was developed by Kotwicki and Lauth (2013) and updated by Conner and Lauth (2017). The index is the two dimensional areal extent of cold benthic waters on the eastern Bering Sea shelf observed during the AFSC summer bottom trawl survey. We used the area (km^2) specified for the isothermal contour intervals < 2°C.

177

178 Since environmental variables often co-vary (e.g., high sea ice concentration is related to an
179 extensive summer cold pool), we evaluated correlations among the variables prior to inclusion as
180 covariates in our age-3 pollock models. Strong correlations ($|r| \geq 0.85$, Table 1) were found
181 among all the environmental variables, so only the cold pool index was included in the statistical
182 analysis of pollock abundance indices. Means of sea surface temperature and cold pool index
183 were graphed to visualize climatic variations during the study period (Fig. 2).

184

185 *2.2.2 Zooplankton collection and processing*

186 Zooplankton samples were collected and analyzed using methods described in Coyle et al.
187 (2011) and Eisner et al. (2014, 2017). Briefly, for the years 2002–2011, samples were collected
188 with a 60-cm bongo frame with 505 µm mesh, towed obliquely from near bottom to the surface.
189 In 2012–2016, depending on taxa, samples were collected with 20 cm/153 µm mesh and 60
190 cm/505 µm mesh nets (Table 2). Volume filtered was measured with a calibrated General
191 Oceanics flowmeter located in the net opening. All zooplankton samples were preserved in 5%
192 formalin buffered with 2% sodium borate and filtered seawater. Samples from 2002–2004 and
193 2012–2016 were sorted at the Polish Plankton Sorting and Identification Center (Szczecin,
194 Poland), samples from 2005–2010 were sorted at the University of Alaska (Coyle et al., 2008),
195 and samples from 2011 were sorted at the NOAA AFSC Auke Bay Laboratories and quality
196 checked by the University of Alaska. Typically, a subsample of 200 organisms was counted from
197 each sample. To estimate number per m^3 at each station for each copepod taxa, counts of each
198 copepod taxa in the subsample were multiplied by the volume of the sample divided by the
199 volume of the subsample, then divided by the volume filtered by the net. We derived integrated

values of catch (b_i) (number m^{-2}) at each station by multiplying the mean abundance (number m^{-3}) by water column depth minus 5 m, the distance nets were deployed off bottom at each station. Biomass data were not included in our analysis, since data were unavailable for several of the years.

Taxa used for the large copepod index include *Calanus* spp., *M. pacifica*, and *Neocalanus* spp. (*N. cristatus*, *N. flemingerii*, *N. plumchrus* and unidentified *Neocalanus* species). These taxa are found primarily over the middle and outer shelf of the eastern Bering Sea during summer (Coyle et al., 2011; Eisner et al., 2014, 2015; Napp et al., 2002; Vidal and Smith, 1986) with higher abundances (*Calanus* spp. in particular) and greater interannual changes observed south of 60°N compared to 60-63°N (Eisner et al. 2014). All 3 taxonomic groups are pelagic and effectively captured with bongo net tows (standard sampling gear) towed through the water column. Abundances for each species include the sum of copepodite stages III-adult for *Calanus* spp. *and Neocalanus* spp., and copepodite stages IV-adult for *M. pacifica*. *Calanus* spp. were primarily copepodite stage V and dominated the large copepod abundances in cold years (Eisner et al., 2014, 2017). The later stages were selected for analysis, since lipid content is higher for large later stage copepods, which in turn, enhances lipid content in their predators (e.g., age-0 pollock) (Heintz et al., 2013). At each station we summed all three taxa to estimate the total large copepod abundance (denoted C+MN), singly evaluated *Calanus* spp. abundance (denoted C), and summed *M. pacifica* and *Neocalanus* spp. abundances (denoted MN). Mean abundances per year for each taxa grouping (C+MN, C, MN) were estimated using all stations sampled. Note that during late summer *M. pacifica* is found in much higher abundance than *Neocalanus* spp., although both are typically located in the outer domain (Eisner et al., 2014, 2017). Although

223 euphausiids are also important diet items for pollock, they were excluded from our analysis since
224 zooplankton tows were collected primarily during the daytime when euphausiids may be
225 concentrated within 1–2 m of the sea floor (Coyle and Pinchuk, 2002), below the reach of our
226 survey nets.
227
228 To evaluate potential bias for changes in mesh size and net diameter over our study period, we
229 compared abundances of *Calanus* spp., *M. pacifica*, and *Neocalanus* spp. collected using two
230 different nets/gears deployed in parallel at the same stations on BASIS surveys, 2006–2010.
231 First, we deployed a vertically towed PairoVet with 25 cm /153 µm mesh, then immediately
232 afterward deployed an obliquely towed bongo net with 60 cm/505 µm mesh. For our
233 comparisons, we evaluated the stages described above, excluding *N. cristatus* CIV-adult since
234 sampling gear did not vary among years for this taxa and stage (Table 2). Paired t-tests using
235 natural log transformed data did not show significant differences in abundances of *Calanus* spp.
236 ($p = 0.74$) or *Neocalanus* spp. ($p = 0.18$), but did show differences for *M. pacifica* ($p < 0.001$).
237 *M. pacifica* median abundances for 505 µm mesh samples were 0.39 times that for 153 µm mesh
238 abundances (95% CI 0.28–0.52), indicating that the 153 µm mesh nets collected over twice as
239 many individuals as the 505 mesh nets. To more accurately examine variations over time, we
240 adjusted the *M. pacifica* data for 2012, 2014–2016 (153 µm mesh samples, Table 2) by
241 multiplying the abundances at each station by 0.39, before we combined abundances of *M.*
242 *pacifica* with *Neocalanus* spp. and *Calanus* spp.
243
244 *2.2.3 Pollock recruitment indices*

Recruitment and survival estimates for the 2002–2015 year classes were acquired from the 2018 pollock stock assessment model for the Bering Sea (Ianelli et al., 2018). Recruitment of pollock to age-3 was represented by stock assessment estimates of the abundance of age-3 pollock (millions of fish) (Ianelli et al., 2018), hereafter referred to as AGE3. Survival of pollock from egg to age-3 was represented by the number of age-3 pollock (millions of fish) per female spawning biomass (SSB, thousands of tonnes) by year class (Ianelli et al., 2018), hereafter referred to as AGE3/SSB. We used the natural log of AGE3/SSB in all analyses.

2.3 Analysis

2.3.1 Estimates of large copepod abundances

We used 1) a sample-based approach and 2) a spatio-temporal model-based approach to estimate the abundance of large copepods (C+MN, C, MN) for our analysis of time series and spatial distribution. The southeastern Bering Sea shelf was chosen for our analysis of copepod abundance because age-0 pollock were located in this region during late summer in both warm and cold years (Eisner et al., 2015).

2.3.1.1 Sample-based indices

For the first approach, copepod data from bongo nets were used to estimate mean abundance over the water column at each station, and then calculate mean abundances by year among stations across our study area, hereafter termed, sample-based indices or estimates. This approach is similar to the one reported in the Alaska Marine Ecosystem Status Report (https://access.afsc.noaa.gov/reem/ecoweb/Index.php) by Eisner and Yasumishii (2017).

2.3.1.2 VAST model-based indices

The second approach was to use a spatio-temporal model to generate model-based copepod indices (spatial distributions and annual mean abundances) from the bongo net samples of large copepods at each station. The model integrates spatial variation in average density across years ("spatial variation") as well as spatial variation for each individual year ("spatio-temporal variation") when estimating large copepod abundance over the BASIS survey area. We used the VAST version 8.2.0 package in R software (Thorson et al., 2016b, c; Thorson and Barnett, 2017) with Microsoft R Open software version 3.5.3 (R Core Team, 2016). Spatial and spatio-temporal variation in the estimates of abundance were included to improve density predictions in areas with few or missing data (Shelton et al., 2014).

Below is a condensed outline of the structure of the VAST model developed by and presented in Thorson et al. (2016a). The VAST model used here is a delta lognormal spatio-temporal model that includes two linear predictors, one for the probability of encounter and the other for positive catch rate probability (Thorson et al., 2015).

An index of population abundance is estimated while integrating density estimates across space. Catch data b_i for each sample i is assumed to follow a probability distribution that includes (i) the probability of encounter $p(s_i, t_i)$ for location s_i, and year t_i and (ii) the expected catch rate $r(s_i, t_i)$, such that expected density $d(s, t)$ is the product of these two terms $d(s, t) = p(s, t)r(s, t)$:

$$\Pr(b_i = B) = \begin{cases} 1 - p(s_i, t_i) & \text{if } B = 0 \\ p(s_i, t_i) \times Lognormal\{B|log[w_i \times r(s_i, t_i)], \sigma^2\} & \text{if } B > 0 \end{cases} \quad (1)$$

where Lognormal$(x|\mu,\sigma^2)$ is a lognormal probability distribution function for *x*, given a log-mean of μ and a variance of σ^2, and w_i is area swept (set at a constant 1 m^2).

Spatio-temporal variation in encounter probability, $p(s_i,t_i)$ was estimated using a logit-linked linear predictor given as:

$$logit[p(s_i,t_i)] = \beta_p(t_i) + \omega_p(s_i) + \varepsilon_p(s_i,t_i) \quad (2)$$

where $\beta_p(t_i)$ is an intercept for encounter probability, $\omega_p(s_i)$ is the spatial variation in encounter probability, $\varepsilon_p(s_i,t_i)$ is the spatio-temporal variation in encounter probability.

Expected catch rates given an encounter $r(s_i,t_i)$ were estimated using a log-linked linear predictor given as:

$$log[r(s_i,t_i)] = \beta_r(t_i) + \omega_r(s_i) + \varepsilon_r(s_i,t_i) \quad (3)$$

where $\beta_r(t_i)$ are the intercepts for expected catch rates, $\omega_r(s_i)$ is the estimated spatial variation in catch rates, and $\varepsilon_r(s_i,t_i)$ is the estimated spatio-temporal variation in catch rates. The probability of encounter intercept and catch rate intercept were estimated as fixed effects.

To approximate the spatial random effects, the stochastic partial differential equation (SPDE) approach was used in a triangulated mesh to approximate the Matérn correlation function, where

nearby sites are more similar to each other. Extrapolated densities within the mesh were at a 42 km resolution.

Total abundance $I(t)$ was predicted by summing density over the entire survey area in each year, t, where this abundance $I(t)$ is then treated as an index of abundance:

$$I(t) = \sum_{s=1}^{n_s}(a(s) \times p(s,t) \times r(s,t)) \quad (4)$$

where $a(s)$ is the area associated with location s (Shelton et al., 2014; Thorson et al., 2015). The prediction grid and thus a(s) was the same for all years. The estimated abundance $I(t)$ of each copepod group was then divided by the extrapolated total survey area (3.57016×10^{11} m^2) to estimate average number of individuals per meter square footprint.

We used the epsilon bias-correction estimator for index $I(s)$ to reduce bias from calculating derived quantities of abundance as a nonlinear function of random effects or high variance in random effects (Thorson and Kristensen, 2016). We used Akaike information criterion (AIC) to determine whether to use a lognormal or gamma distribution for observation error in positive catch rates. Output from the C and MN models were summed to provide a C+MN index.

Model performance was examined by comparing the expected probability and observed frequency of encounter for encounter probability, actual versus predicted plots of the encounter probability, and quantile-quantile (Q-Q) plots for the residuals of the positive catch rates, and spatial trends in the Pearson residuals for encounter probability and positive catch rate

components by knot (Figs. S.2 - S.9). A 10-fold cross validation was conducted to test model performance using simple random sampling with replacement. For each of 10 cross validation experiments, we excluded 10% of the data, fitted the model to the remaining 90%, and then predicted observations for the 10% that were excluded. We then computed the probability of those excluded data given the model fits. To evaluate predictive performance, we compared the predicted values from the full sample with those generated from the 10-fold cross validations. Plots were made of the observed values versus predicted values for the full sample (in-sample) and for the cross validation (out-of-sample) analyses (Fig. S.10). Code to implement this cross validation experiment is based upon sample code that is publicly available online (https://github.com/James-Thorson-NOAA/VAST/wiki/Crossvalidation).

2.3.1.3 Sample–based vs VAST model-based areal coverage and magnitude

To estimate annual means, sample-based data were averaged (including zeros) over the area sampled in a given year, whereas VAST model-based indices was averaged over the same area every year. Since this area encompasses observations across all years, it is larger than or equal to the sample-based area for a given year since the size of the survey area varied among years as described earlier, but is expected to result in a more comparable copepod abundance index across time and spatial extent of survey effort. The VAST model-based outputs provided a relative index of abundance. While absolute values cannot be directly compared with the sample-based means, the relative (proportionate) interannual variations and patterns over time are useful to examine.

To evaluate and compare spatial patterns, we produced heat maps of the standardized sample-based and the VAST model-based copepod densities ln([number km^{-2}]+1) to show the distributions over the survey area for each year. Prior to plotting, the separate data sets were standardized by subtracting the mean and dividing by the standard deviation. For both the sample-based and VAST model-based data, heat maps were generated using the gridded bivariate linear interpolation for irregular data using the interp function in the akima R package (version 0.6-2).

2.3.2 Relationships of pollock indices to copepod abundance and cold pool index

Least squares linear regressions were used to evaluate and visualize the relationships between response variables (pollock indices) and predictors (copepod indices or the environmental variable, cold pool index, from when the pollock were age-0). Pollock indices include: AGE3 or ln(AGE3/SSB), and copepod indices include C+MN, C, and MN from sample-based and VAST model-based estimates. Separate models were run for each predictor. The relationship between ln(AGE3/SSB) and predictors, can be described as linearized Ricker spawner-recruit models (Ianelli et al., 2018; Ricker, 1975), therefore, we included SSB as a predictor (to account for density dependence) in these models (Table 3). The models for AGE3 were similar but did not include log transformations or SSB. For all regressions, residuals were tested for 1st order autocorrelation (forecast package version 5.8 in R). If present, then we added a term for 1st order autocorrelation as a predictor in the model. The Shapiro-Wilks test was used to test for normality of the residuals. There were no significant autocorrelation in the residuals so there was no need to add an autocorrelation term to the regression models. AGE3 estimated from the linear regression models using VAST model-based copepod indices (C+MN) also were compared

381 directly with AGE3 stock assessment estimates for 2002–2015. For the 2016 year class,
382 predictions of AGE3 were estimated using the relationship between C+MN and AGE3 for the
383 prior years.
384
385 To evaluate if copepod and cold pool indices combined provided a better estimation of AGE3
386 and ln(AGE3/SSB), we used a stepwise multiple linear regression analysis using backward
387 elimination with an F-to-remove statistic of 4 (corresponding to a T value of 2 and tail
388 probability value of ~ 0.05). This F-statistic was used for testing the significance of a regression
389 coefficient and subsequently removed any coefficients where the F-statistic was below 4. Linear
390 regressions were run using SYSTAT version 13.2. The best fit model was the one resulting from
391 backward elimination until no further variables could be removed without a statistically
392 significant loss of model fit.
393
394 3. Results

395 We describe changes in the environment over the study period, then describe variations in
396 copepod abundance interannually and spatially using sample-based and VAST model-based
397 indices and compare results from these two methods. Finally, we estimate the pollock indices
398 from copepod indices, from the cold pool index, and from the combination of both.
399

400 **3.1 Interannual variations in environmental indices**

401 An examination of the interannual variations in key environmental drivers important to growth
402 and survival of large copepods and pollock helps to characterize mechanisms driving the
403 observed changes in abundances. Time series (2002–2016) of sea surface temperature and the

cold pool index (highly correlated with sea ice extent, Table 1) indicate that in warm years, sea surface temperature was ~2–3°C higher, while the cold pool area was a third of the size compared to cold (high ice) years (Fig. 2).

3.2 Large copepod abundance variations

3.2.1 Time Series

3.2.1.1 Sample-based indices

Sample-based mean abundances of large copepods indicate that abundances of all three taxa combined (C+MN), *Calanus* spp. (C) alone, and *M. pacifica* +*Neocalanus* spp. (MN) were high in cold years and low in warm years (Figs. 2, 3). Note that *Calanus* spp. largely drives the abundance variations for C+MN as evidenced by the high correlation between these indices (Table 1). The highest values for C+MN and C were seen in 2012, the year with the greatest cold pool extent for the study period.

3.2.1.2 VAST model-based indices

VAST model parameters and diagnostics are reported in the Supplementary Material. The C model had significant year, spatial, and spatio-temporal effects in both the encounter probability and positive catch rates given an encounter (Table S.1). The MN model had significant spatial variation in the probability of encounter, and significant year, spatial, and spatio-temporal effects in positive catch rates given an encounter. The C and MN models were specified as having a lognormal distribution rather than a gamma distribution (based on lowest AIC) on positive catch rates and a conventional delta-model, but fixing encounter probability = 1 for any year where all samples encounter the species (Tables S.1, S.2). VAST model diagnostics (Figs. S.2-S.9)

indicate a relatively good model fit for both C and MN. Expected probability and observed frequency of encounter for encounter probability component were within the 95% predictive interval, although patterns in the residuals for the encounter probability for C indicate some evidence of underdispersion. Q-Q plot of residuals for positive catch rate component for the models were along the diagonal line indicating normal distribution of the residuals.

Cross validation plots for C and MN estimates from VAST models are shown in Figure S.10. Observed vs. predicted positive catch rate relationships were similar for the in-sample and out-of-sample data from the 10-fold cross validation indicating good model performance for each model. There is some evidence for overprediction of small catches and underprediction of large catches, however all of the age-3 pollock predictions were within one standard deviation (see Figs. S2, S6). In all plots, predicted values were higher than observed values at lower observed zooplankton densities. There appears to be less variability around the relationship between observed versus predicted values for the C than the MN models.

VAST model-based indices followed the same general pattern as the sample-based means for C+MN and C, although 2008 means were higher relative to other years than seen for sample-based data (Fig. 3). VAST model-based indices for the MN group were higher than sample-based values with large and opposite differences in 2008; removal of 2008 from our analysis produced more similar patterns with an r of 0.60 ($p = 0.039$), compared to $r = -0.26$ ($p > 0.05$) for the entire study period (Table 1).

3.2.2 Spatial distribution

450 3.2.2.1 Sample-based indices

451 Higher standardized abundances of C were found on the outer shelf than on the middle shelf in
452 warm years (with the exception of 2014, the first warm year after the cold stanza ended), while
453 distributions were extended over the middle and outer shelf or were concentrated on the middle
454 shelf (e.g., 2012) in cold years (Fig. 4a). MN typically had the highest standardized abundance
455 on the outer shelf, with patches of moderate abundance seen further inshore in many years (Fig.
456 5a).

457

458 3.2.2.2 VAST model-based indices

459 Broad scale spatial patterns among years was generally similar for VAST model-based indices
460 and sample-based indices for standardized C data (Fig. 4), although in the VAST plots, the cross-
461 shelf and interannual variations appear larger. For standardized MN data, the highest abundances
462 from VAST were consistently seen in outer shelf waters, but extensions inshore did not always
463 match up with the sample-based data; similar to C, cross-shelf variations appear larger for VAST
464 output (Fig. 5).

465

466 **3.3 Relationships of pollock indices to copepod abundance and cold pool index**

467 Sample-based mean copepod abundances were found to have significant ($p < 0.05$) linear
468 relationships with AGE3 for C+MN and C ($R^2 = 0.43$ and 0.44, respectively), but not for MN (p
469 $= 0.29$) (Fig.6). Strong relationships was found for ln(AGE3/SSB) with SSB and sample-based
470 C+MN or C covariates included ($R^2 = 0.68$, for both), however inclusion of MN with SSB did
471 not improve the fit over SSB alone (Table 3).

472

473 VAST model-based copepod indices (C+MN, C, and MN) were significantly linearly related to
474 AGE3 (R^2 = 0.74, 0.62, and 0.49, respectively, Fig. 6) and to ln(AGE3/SSB) with SSB included
475 as a covariate (R^2 = 0.75, 0.71, and 0.67, respectively, Table 3). All linear relationships were
476 stronger for VAST modeled copepod data compared to means derived from sample-based data.
477 In particular, the increase in copepod mean abundances in 2008 in the VAST model-based
478 indices contributed to the stronger linear fits with AGE3 (Fig. 6). Predictions for AGE3 for the
479 2016 year class (estimates for age-3's recruited into fishery in 2019) based on VAST model-
480 based estimates of copepods (C+MN), suggested pollock recruitment would be low (Fig. 7).
481
482 Pollock indices were significantly linearly related to the cold pool index (during the age-0
483 pollock stage), as shown in Figure 8 for AGE3 (R^2 = 0.56) and Table 3 for ln(AGE3/SSB) (R^2 =
484 0.77). Multiple stepwise linear regressions with sample-based copepod indices and the cold pool
485 index as covariates, identified the cold pool index alone as the best estimator of AGE3 (Table 4).
486 In contrast, regressions with VAST indices indicated the copepod indices were the best
487 estimators of AGE3, with the exception of the addition of the cold pool to MN. The
488 ln(AGE3/SSB) was best described as a function of the cold pool index alone, except for the case
489 when the VAST model-based MN and cold pool indices were combined (Table 4).
490
491 4. Discussion
492 A key finding was the strong relationship between the mean abundance of large copepods
493 (largely driven by changes in *Calanus* spp.) and recruitment of pollock into the fishery three
494 years later; this relationship was improved using VAST spatio-temporal modeling estimates of
495 copepod abundance, relative to simply calculating means among stations from spatially

496 unbalanced survey data. These findings provide an excellent basis for further research into
497 recruitment modeling. In general, during late summer on the southeastern Bering Sea shelf, large
498 copepods were in higher abundances in bongo nets and in age-0 pollock diets (Andrews et al.,
499 2016; Coyle et al. 2011), and more broadly distributed in cold, high-ice years than in warm, low-
500 ice years. Decreases in the availability of these lipid-rich prey during warm years may prove
501 detrimental to the pollock recruitment into the fishery at age-3 as well as impacting other fish
502 and higher trophic level consumers (e.g., seabirds) (Hunt et al., 2011; Sigler et al., 2016).
503 Therefore, this information is important for fisheries and ecosystem management.
504
505 The findings for our time series of zooplankton abundance in the eastern Bering Sea have
506 important implications. Similar to prior analysis of 2003–2009 data (Eisner et al., 2014), large
507 copepod abundances for our extended time series, 2002–2016, indicate that *Calanus* spp. were
508 located in the outer shelf in low numbers in warm years (with the exception of 2014) and more
509 broadly distributed over the middle and outer shelf in high numbers in cold years. Recall that
510 2002–2005 and 2014–2016 were warm, low-ice years, while 2007–2012 were cold, high-ice
511 years, and 2006 and 2013 were considered "average" years. Abundances of *Calanus* spp. may
512 not decrease until one year after the start of a warm stanza, similar to delays in increased
513 abundance observed for the start of a cold year stanza, e.g., the first cold year was 2007, while
514 the largest increase was noted in 2008 (Fig. 3; Eisner et al., 2014). Higher abundances of large
515 copepods also were collected in July and September in cold (2007–2011) compared to warm
516 (2001–2005) stanzas along the 70-m isobath in the southeastern Bering Sea (Kimmel et al.,
517 2017). These authors similarly concluded that variations in sea-ice extent drive changes in
518 copepod abundances, and the greatest impacts to upper trophic levels were driven by

519 July/September copepod production rates, with significantly higher estimated rates for *Calanus*
520 spp. in cold than warm years.
521
522 Our results demonstrate, that *Calanus* spp., the taxa driving abundance changes of C+MN,
523 expand distributions to the outer shelf and cover a larger area in cold years (~50-180 m
524 bathymetry) compared to warm years (~50-100 m bathymetry). This change in distribution in
525 addition to increases in mean abundance in cold years can add to increased overlap between age-
526 0 pollock and lipid-rich zooplankton prey, as demonstrated for 2010 (cold year) compared to
527 2005 (warm year) in the southeastern Bering Sea (Siddon et al., 2013). In mid-summer,
528 concentrations have been observed to drop off at the shelf-break (Eisner et al., 2017). This is not
529 surprising since *Calanus* spp. is thought to diapause on the shelf (Coyle and Gibson, 2017), and
530 therefore, would remain on the shelf over its entire life cycle.
531
532 The abundance of age-0 pollock and subsequent abundances of age-1 and age-3 pollock for a
533 given year class do not appear to be positively correlated in the eastern Bering Sea (McKelvey
534 and Williams, 2018; Moss et al., 2009; Parker-Stetter et al., 2013). Abundances of age-0 pollock
535 in surface waters (top 20 m) from BASIS were high in warm years 2004 and 2005, and low in
536 cooler years 2006 and 2007 (Moss et al., 2009). This is unlike the stock assessment trends for
537 age-3 pollock with high abundances in 2006 and lower abundances the other 3 years (particularly
538 2004, Fig. 7). Pollock year classes with high abundances of age-0s were observed to have low
539 abundances of age-1 pollock (low over winter survival) and vice versa (Moss et al., 2009).
540 Acoustic data collected on BASIS surveys for estimation of age-0 pollock over the water column
541 indicated that abundances in 2014 were 9 times higher than observed in 2011 and 3.5 times

542 higher than in 2012 (McKelvey and Williams, 2018). In contrast, age-3 pollock abundances were
543 low and similar for 2011 and 2014 year classes with very high abundances for 2012. Similar
544 discrepancies were found between age-0 and age-3 pollock abundances for acoustic data
545 evaluated for 2009 and 2010 (Parker-Stetter et al., 2013).
546
547 The health of the age-0 fish at the end of summer appears to be a better predictor than abundance
548 for over winter survival. The percent of large copepods (dominated by *Calanus* spp.) in age-0
549 pollock diets is higher in cold years (Coyle et al., 2011; Andrews et al., 2016), and aligns with
550 years when age-0 pollock had higher energy reserves (kJ/g) in late summer, higher overwinter
551 survival and higher recruitment of age-1 and age-3 fish (Heintz et al., 2013; Sigler et al., 2016).
552 Accordingly, the spatial and temporal overlap of age-0 pollock with lipid-rich zooplankton is
553 also critical for survival (Siddon et al., 2013).
554
555 Other pollock studies in the eastern Bering Sea also have related physical and biological
556 variables during the age-0 and age-1 life stages to recruitment to older ages. Cannibalism, as
557 indexed by separation of the adults and juveniles based on an ocean current model, was found
558 important in determining pollock survival (Wespestad et al., 2000). Yasumiishi et al. (2015)
559 found a positive relationship between the event of a cooler summer during the age-0 stage
560 (optimal conditions for lipid-rich prey) followed by a warmer spring (earlier spring bloom for
561 first feeding) and recruitment of pollock to age-3. Growth in body weight of chum salmon
562 (*Oncorhynchus keta*) during the age-0 life stage of pollock was used as a proxy for ocean
563 conditions and linked to higher recruitment of pollock to age-3 (Yasumiishi et al., 2015).
564

565 The relationship between large copepods and age-3 pollock abundances was improved using the
566 copepod indices from the VAST spatio-temporal model particularly for years when sampling
567 was limited. For example, the VAST model-based indices compared to sample-based indices
568 predicted a higher abundance of large copepods in 2008, a year when the sample coverage did
569 not extend into the outer shelf. The outer shelf is where *M. pacifica* and *Neocalanus* spp. are
570 found in the highest concentrations and where *Calanus* spp. are often observed in high numbers
571 (Figs. 4, 5). Consistently using the VAST model to estimate distributions over the outer shelf,
572 where sampling is often more limited, may be important for understanding interannual variations
573 in *M. pacifica* and *Neocalanus* spp. This may partially explain why linear relationships with age-
574 3 pollock abundances are only significant for VAST model-based indices of *M. pacifica* +
575 *Neocalanus* spp. However, we note that when VAST extrapolates into unsampled regions or
576 years, the variances around those density estimates are inflated and this increased variance in
577 abundance indices will likely lead to reduced correlation in those extrapolations, and
578 subsequently increased variability around the expected correlation coefficient.
579
580 The positive correlations between the *M. pacifica* + *Neocalanus* spp. VAST model-based index
581 and age-3 pollock abundances or age-3 abundance/spawning stock biomass may reflect
582 ecological processes that occurred prior to the survey (spring or early summer) as well as during
583 the survey period. *Neocalanus* spp. abundances are highest in spring when they are advected
584 onto the shelf as early copepodite stages followed by stage progression and growth to copepodite
585 stage V, with downward migration starting in late spring/early summer (Smith and Vidal, 1986;
586 Vidal and Smith, 1986). For example, maximum biomass of *N. plumchrus* was obtained by late
587 May/early June followed by descent of a significant fraction into deep water (> 80 m) (Vidal and

588 Smith, 1986). Eisner et al. (2017) observed that *N. cristatus* mean abundances were relatively
589 high in April/May, moderate in June/July and low in September. However, some portion must
590 remain accessible to forage fish and seabirds during the summer since *Neocalanus* spp. have
591 been commonly observed in age-0 pollock diets in August-September on the southeastern shelf
592 (Moss et al., 2009; Siddon et al., 2013) and in least auklet (*Aethia pusilla*) diets July-August on
593 the Pribilof Islands (Dorresteijn et al., 2012). In addition to higher abundances of *Neocalanus*
594 spp. in cold years, retention times on the shelf may be longer in cold compared to warm years
595 (Dorresteijn et al., 2012). For *M. pacifica*, abundances in 2008-2010, were shown to increase in
596 June, peak in July and taper off substantially by August and September (Eisner et al., 2017). Diet
597 studies for 2008 indicated that *M. pacific*a (early and late stage) were important prey for pollock
598 larvae in spring (May) (Strasburger et al., 2014).
599
600 The age-3 abundance/spawning stock biomass index, ln(AGE3/SSB), was included in our
601 analyses to evaluate the importance of maternal effects and density-dependent effects of
602 spawning biomass on survival. Density dependence has been observed for Bering Sea pollock
603 stocks in prior research (Mueter et al., 2011). Strong density-dependent effects of spawning
604 biomass on survival indicate competition among juveniles, cannibalism among juveniles and
605 cannibalism on juveniles by adults (Dwyer et al., 1987). Our regression models predicting
606 ln(AGE3/SSB) as a function of spawning stock biomass and cold pool area or large copepod
607 abundance suggests that survival can be explained by the direct effects of density dependence,
608 indirect effects of environment on density-dependence, or by environment and prey indices, such
609 as large copepods. Environmental factors may have a larger influence on recruitment than
610 spawning biomass for many fisheries stocks (Maunder and Thorson, this issue).

611

612 The strong linear relationships found between the environmental covariate and large copepod
613 and pollock indices demonstrate the importance of regional regime changes, related to
614 atmospheric forcing (e.g., Aleutian Low), on the Bering Sea ecosystem. The high correlations for
615 large copepod indices with sea ice cover, cold pool areal extent, bottom temperature and to a
616 lesser extent sea surface temperature (Table 2) are not surprising, and have been found to be
617 important in prior analysis of large zooplankton in this region (Eisner et al., 2014; Sigler et al.,
618 2016). For age-3 pollock abundance and abundance per spawning stock biomass, the high
619 correlations with the cold pool area three years prior ($R^2 = 0.56$ and 0.77, respectively) is less
620 well established. Although correlations of age-3 pollock abundance were higher with VAST
621 model-based large copepod indices ($R^2 = 0.74$ for the three groups combined), these
622 environmental indicators (in particular, cold pool area) from the age-0 year, could aid in
623 estimations of age-3 pollock abundance if large copepod data are unavailable. Future work could
624 develop a multivariate model that jointly models spatial variation in copepod density and
625 environmental variables (e.g., sea ice extent and water temperature); this model could then be
626 used to inform estimates of copepod density in unsampled areas based on their correlation with
627 environmental variables that are typically measured across a larger spatial extent.
628

629 The purpose of the models presented here is to produce model-based indices of copepod
630 abundance to then use this information, as well as oceanographic conditions, to establish a link
631 between relative abundances of plankton and pollock. In our proof of concept here, we've
632 demonstrated that this can be effectively done and that copepod abundance can be used to
633 represent the abundances of age-3 pollock in the near future. In this study, the encounter

probability model for C was underdispersed. In terms of the application of this model to management, this is potentially an issue when there are extremely low levels of copepods and the model could potentially overpredict C abundance. This then potentially biases future age-3 pollock numbers upward. We therefore encourage future work to develop an improved observation model for the C encounter probability. We also encourage the implementation of this proof of concept study by considering (1) the use of multiple status indicators at once (e.g., an ensemble of indicators) as is done with many climatological studies that average over models to deal with model misspecification, (2) the development and incorporation of more complex likelihood functions to better fit the observation data, and (3) the uncertainty around estimates of copepods and age-3 pollock abundances to provide a distribution of R^2 values for regressions (potentially using an error-in-variables modelling approach or hierarchical model). These additional analyses would provide support for the use of copepod abundance as an early indicator for pollock recruitment success for management purposes.

Our large copepod index for prediction of age-3 pollock recruitment exemplifies the importance of the conditions during the first year at sea to growth and survival of pollock in the eastern Bering Sea (Sigler et al., 2016). An understanding of the mechanisms driving the survival of fish during this critical stage is the basis for our predictions. In this case, pollock overwinter survival appears to be at least partially tied to the availability of lipid-rich zooplankton prey during the first summer at sea, which in turn are enhanced by the presence of sea ice during the prior winter/spring. Sea ice provides an early food source for these zooplankton in the form of ice algae or ice-associated phytoplankton (Baier and Napp, 2003; Wang et al., 2015). Additionally, the lower water temperature in high ice years reduces metabolic requirements for these

zooplankton, so they require less food to survive (Coyle and Gibson, 2017). These mechanistic processes might be useful for management of other eastern Bering Sea fisheries besides pollock (e.g., juvenile Pacific cod (*Gadus macrocephalus*) had lower growth potential, calculated from prey energy density and temperature, in a warm year compared to a cold year, Hurst et al., 2018), or may be applicable to other subarctic or arctic ecosystems with large variations in seasonal sea ice. The relationships we have developed between large copepods, environmental variables and age-3 pollock indices could be incorporated into ecosystem models to predict abundance and production of higher trophic level organisms as climate change progresses and baselines shift. Finally, the copepod and cold pool indices could also be incorporated as an index of cohort strength in the pollock stock assessment model, and its importance relative to other drivers of pollock demographics could be assessed using a growing toolbox of stock assessment techniques.

Acknowledgements

We thank the staff and crew of the fisheries oceanography research vessels: *Oscar Dyson, Sea Storm*, *Northwest Explorer*, *Epic Explorer* and *Bristol Explorer* for assistance with zooplankton collection over many years. We are grateful for the assistance in field sampling, data processing and analysis from NOAA scientific staff and volunteers. Numerous scientists from outside NOAA (e.g., TINRO, UAF, DFO) also assisted with this large data collection effort. We thank K. Coyle and his lab for assistance and guidance on BASIS zooplankton sampling and analysis, as well as the Polish Plankton Sorting and Identification Center for their contributions for the more recent (2012-2016) zooplankton data. Funds were provided by the North Pacific Research Board and NOAA/NMFS/Alaska Fisheries Science Center. We deeply appreciate reviews by J.T.

680 Thorson and G.L. Hunt on earlier drafts of this manuscript and reviews from three anonymous
681 reviewers.

682 References

683 Andrews, A.G., Siddon, E.C., Auburn-Cook, M., 2016. A new index of age-0 Walleye Pollock
684 prey quality provides a leading indicator of energetic content In: Zador. S. (Ed.),
685 Ecosystem Considerations for 2016. Appendix C of the BSAI/GOA Stock Assessment
686 and Fishery Evaluation Report. Technical report, North Pacific Fishery Management
687 Council, 605 W. 4th Ave., Suite 306, Anchorage, AK 99501.

688 Baier, C.T., Napp, J.M., 2003. Climate-induced variability in *Calanus marshallae* populations. J.
689 Plankton Res. 25, 771–782.

690 Brodziak, J., O'Brien, L., 2005. Do environmental factors affect recruits per spawner anomalies
691 of New England groundfish? ICES J. Mar. Sci. 62(7), 1394–1407.
692 https://doi.org/10.1016/j.icesjms.2005.04.019.

693 Buckley, T.W., Ortiz, I., Kotwicki, S., Aydin, K., 2016. Summer diet composition of walleye
694 pollock and predator–prey relationships with copepods and euphausiids in the eastern
695 Bering Sea, 1987–2011. Deep Sea Res. II. 134, 302–311.

696 Coachman, L.K., 1986. Circulation, water masses and fluxes on the southeastern Bering Sea
697 shelf. Cont. Shelf Res. 5, 23-108.

698 Conner, J., Lauth, R.R., 2017. Results of the 2016 eastern Bering Sea continental shelf bottom
699 trawl survey of groundfish and invertebrate resources. U.S. Department of Commerce,
700 NOAA Technical Memorandum NMFS-AFSC-352, 159 p.

701 Coyle, K.O., Pinchuk, A.I., 2002. Climate-related differences in zooplankton density and growth
702 on the inner shelf of the southeastern Bering Sea. Prog. Oceanogr. 55, 177–194.

703 Coyle, K.O., Pinchuk, A.I., Eisner, L.B., Napp, J.M., 2008. Zooplankton species composition,
704 abundance and biomass on the eastern Bering Sea shelf during summer: the potential role

of water column stability and nutrients in structuring the zooplankton community. Deep Sea Res. II. 55, 1775–1791.

Coyle K.O., Eisner, L.B., Mueter, F.J., Pinchuk, A.I., Janout, M.A., Cieciel, K.D., Farley, E.V., Jr., Andrews, A.G., 2011. Climate change in the southeastern Bering Sea: impacts on pollock stocks and implications for the oscillating control hypothesis. Fish. Oceanogr. 20(2), 139–56.

Coyle, K.O. Gibson, G.A., 2017. *Calanus* on the Bering Sea shelf: probable cause for population declines during warm years. J. Plankton Res. 39(2), 257–270. https://doi.org/10.1093/plankt/fbx005.

Dorresteijn, I., Kitaysky, A.S., Barger, C., Benowitz-Fredericks, Z.M., Byrd, G.V., Schultz, M., Young, R., 2012. Climate affects food availability to planktivorous least auklets *Aethia pusilla* through physical processes in the southeastern Bering Sea. Mar. Ecol. Prog. Ser. 454, 207–220.

Dwyer, D.A., Bailey, K.M., Livingston, P.A., 1987. Feeding habits and daily ration of walleye pollock (*Theragra chalcogramma*) in the eastern Bering Sea, with special reference to cannibalism. Can. J. Fish. Aquat. Sci. 44, 1972–1984.

Eisner, L.B., Napp, J.M, Mier, K., Pinchuk, A.I., Andrews A., 2014. Climate-mediated changes in zooplankton community structure for the eastern Bering Sea. Deep Sea Res II. 109, 157–171. https://doi.org/10.1016/j.dsr2.2014.03.004.

Eisner, L.B., Siddon, E., and Strasburger, W., 2015. Spatial and temporal changes in assemblage structure of zooplankton and pelagic fish across varying climate conditions in the eastern Bering Sea. Izvestia TINRO, 181, 141–160.

727 Eisner, L.B., Pinchuk, A.I., Kimmel, D., Mier, K., Harpold, C. Siddon, E.C., 2017. Seasonal,
728 interannual, and spatial patterns of community composition over the eastern Bering Sea
729 shelf in cold years. Part I: Zooplankton. ICES J. Mar Sci.
730 https://doi.org/10.1093/icesjms/fsx156.
731 Eisner, L.B., Yasumiishi, E.M., 2017. Large copepod abundance as an indicator of pollock
732 recruitment to age-3 in the southeastern Bering Sea. In: S. Zador. S. (Ed.), Ecosystem
733 Considerations for 2017. Appendix C of the BSAI/GOA Stock Assessment and Fishery
734 Evaluation Report. Technical report, North Pacific Fishery Management Council, 605 W.
735 4th Ave., Suite 306, Anchorage, AK 99501.
736 Fissel, B., Dalton, M., Garber-Yonts, B., Haynie, A., Kasperski, S., Lee, J., Lew, D., Lavoie, A.,
737 Seung, C., Sparks, K., 2017. Stock Assessment and Fishery Evaluation Report for the
738 Groundfish Fisheries of the Gulf of Alaska and Bering Sea/Aleutian Island Area:
739 Economic Status of the Groundfish Fisheries off Alaska, 2016, NPFMC, December,
740 2017. http://www.afsc.noaa.gov/refm/docs/2017/economic.pdf.
741 Heintz, R.A., Siddon, E.C., Farley, E.V., Napp, J.M., 2013. Correlation between recruitment and
742 fall condition of age-0 pollock (*Theragra chalcogramma*) from the eastern Bering Sea
743 under varying climate conditions. Deep Sea Res. II. 94, 150–156.
744 Hunt G.L., Stabeno P.J., 2002. Climate change and the control of energy flow in the southeastern
745 Bering Sea. Prog. Oceanogr. 55, 5–22.
746 Hunt, G.L., Coyle, K.O., Eisner, L.B., Farley, E.V., Heintz, R.A., Mueter, F.J., Stabeno, P.J.,
747 2011. Climate impacts on eastern Bering Sea foodwebs: a synthesis of new data and an
748 assessment of the Oscillating Control Hypothesis. ICES J. Mar. Sci. 68(6), 1230–1243.
749 doi:10.1093/icesjms/fsr036.

Hurst, T.P., Miller, J.A., Ferm N, Heintz, R.A., Farley, E.V., 2018. Spatial variation in potential and realized growth of juvenile Pacific Cod in the southeastern Bering Sea. Mar. Ecol. Prog. Ser. 590, 171–185. https://doi.org/10.3354/meps12494.

Ianelli, J.N., Kotwicki, S., Honkalehto, T., McCarthy, A., Stienessen, S., Holsman, Siddon, E.C., K., Fissel, B., 2018. Assessment of walleye pollock stock in the Eastern Bering Sea, in: Stock Assessment and Fishery Evaluation Report for the Groundfish Resources of the Bering Sea/Aleutian Islands Regions. Anchorage: North Pacific Fisheries Management Council.

Iverson, R.L., Coachman, L.K., Cooney, R.T., English, T.S., Goering, J.J., Hunt, G.L., McCauley, M.C., McRoy, C.P., Reeburg, W.S., Whitledge, T.E., 1979. Ecological significance of fronts in the southeastern Bering Sea, in: Livingston. R.J. (Ed.), Ecological Processes in Coastal and Marine Systems, Plenum Press, pp. 437–466.

Kimmel, D., Eisner, L.B., Wilson, M, Duffy-Anderson, J., 2017. Copepod dynamics across warm and cold periods in the eastern Bering Sea: implications for walleye pollock (*Gadus chalcogrammus*) and the Oscillating Control Hypothesis. Fish. Oceanogr. 00, 1–16. doi:10.1111/fog.12241.

Kotwicki, S., Lauth, R.R., 2013. Detecting temporal trends and environmentally-driven changes in the spatial distribution of bottom fishes and crabs on the eastern Bering Sea shelf. Deep Sea Res. II. 94, 231–243. https://doi.org/10.1016/j.dsr2.2013.03.017.

Maunder, M.N., Thorson, J.T. *this issue*. Modeling temporal variation in recruitment in fisheries stock assessment: a review of theory and practice.

771 McKelvey and Williams, 2018. Abundance and distribution of age-0 walleye pollock in the
772 eastern Bering Sea shelf during the Bering Arctic Subarctic Integrated Survey (BASIS) in
773 2014, 48 p. NTIS No.PB2018-101437.
774 Moss, J.H., Farley, E.V., Feldmann, A.M., Ianelli, J.N., 2009. Spatial distribution, energetic
775 status, and food habits of eastern Bering Sea age-0 Walleye Pollock. Trans. Am. Fish.
776 Soc. 138, 497–505.
777 Mueter, F.J., Bond, N.A., Ianelli, J.N., and Hollowed, A.B., 2011. Expected declines in
778 recruitment of walleye pollock (*Theragra chalcogramma*) in the eastern Bering Sea
779 under future climate change. ICES J. Mar. Sci. 68, 1284–1296.
780 Myers, R.A. 2001. Stock and recruitment: generalizations about maximum reproductive rate,
781 density dependence, and variability using meta-analytic approaches. ICES J. Mar. Sci.
782 58, 937–951.
783 Napp, J.M., Hunt, G.L., 2001. Anomalous conditions in the southeastern Bering Sea, 1997:
784 linkages among climate, weather, ocean, and biology. Fish. Oceanogr. 10, 61–68.
785 Napp, J.M., Baier, C.T., Brodeur, R.D., Coyle, K.O., Shiga, N., Mier, K., 2002. Interannual and
786 decadal variability in zooplankton communities of the southeast Bering Sea shelf, Deep
787 Sea Res. II. 49 (26), 5991–6008. https://doi.org/10.1016/S0967-0645(02)00330-2.
788 Parker-Stetter, S., Horne, J., Farley, E., Barbee, D., Andrews, A., Eisner, L., Nomura, J., 2013.
789 Summer distributions of forage fish in the eastern Bering Sea. Deep Sea Res. II. 94, 211-
790 230. https://doi.org/10.1016/j.dsr2.2013.04.022.
791 R Core Team. 2016. R: A language and environment for statistical computing. R Foundation for
792 Statistical Computing, Vienna, Austria. https://www.R-project.org/.

793 Ricker, W.E., 1975. Computation and interpretation of biological statistics of fish populations.
794 Bulletin of Fisheries Research Board Canada 191.
795 Shelton, A.O., Thorson, J.T., Ward, E.J., Feist, B.E., 2014. Spatial semiparametric models
796 improve estimates of species abundance and distribution. Can. J. Fish. Aquat. Sci. 71,
797 1655–1666. https://doi.org/10.1139/cjfas-2013-0508.
798 Siddon, E.C., Kristiansen, T., Mueter, F.J., Holsman, K.K., Heintz, R.A. 2013. Spatial match-
799 mismatch between juvenile fish and prey provides a mechanism for recruitment
800 variability across contrasting climate conditions in the eastern Bering Sea. PLoS ONE.
801 8(12), e84526. https://doi.org/10.1371/journal.pone.0084526.
802 Sigler, M.F., Napp, J.M., Stabeno, P.J., Heintz, R.A., Lomas, M.W., Hunt, G.L., 2016. Variation
803 in annual production of copepods, euphausiids, and juvenile Walleye Pollock in the
804 southeastern Bering Sea. Deep Sea Res. II. 134, 223–234.
805 Smith, S.L., Vidal, J., 1986. Variations in the distribution, abundance, and development of
806 copepods in the southeastern Bering Sea in 1980 and 1981. Cont. Shelf Res. 5, 215–239.
807 https://doi.org/10.1016/0198-0149(86)90129-9.
808 Stabeno, P.J., Napp, J.M., Mordy, C., Whitledge, T., 2010. Factors influencing physical structure
809 and lower trophic levels of the eastern Bering Sea shelf in 2005: sea ice, tides and winds.
810 Prog. Oceanogr. 85 (3-4), 180–196.
811 Stabeno, P.J., Kachel, N.B., Moore, S.E., Napp, J.M., Sigler, M., Yamaguchi, A., Zerbini, A.N.,
812 2012. Comparison of warm and cold years on the southeastern Bering Sea shelf and some
813 implications for the ecosystem. Deep Sea Res. II. 65–70, 31–45.

814 Strasburger, W.W., Hillgruber, N., Pinchuk, A.I., Mueter, F.J., 2014. Feeding ecology of age-0
815 Walleye Pollock (*Gadus chalcogramma*) and Pacific Cod (*Gadus macrocephalus*) in the
816 southeastern Bering Sea. Deep Sea Res. II. 109, 172–180.
817 Thorson, J.T., Shelton, A.O., Ward, E.J., Skaug, H.J., 2015. Geostatistical delta-generalized
818 linear mixed models improve precision for estimated abundance indices for West Coast
819 groundfishes. ICES J. Mar. Sci. 72(5), 1297–1310.
820 https://doi.org/10.1093/icesjms/fsu243.
821 Thorson, J.T., Kristensen, K., 2016. Implementing a generic method for bias correction in
822 statistical models using random effects, with spatial and population dynamics examples.
823 Fish. Res. 175, 66–74. https://doi.org/10.1016/j.fishres.2015.11.016.
824 Thorson, J.T., Ianelli, J.N., Larsen, E.A., Ries, L., Scheuerell, M.D., Szuwalski, C., Zipkin, E.F.,
825 2016a. Joint dynamics species distribution models: a tool for community ordination and
826 patio-temporal monitoring. Global Ecol. Biogeogr. 1–15.
827 https://doi.org/10.1111/geb.12464.
828 Thorson, J.T., Pinsky, M.L., Ward, E.J., 2016b. Model-based inference for estimating shifts in
829 species distribution, area occupied and centre of gravity. Methods Ecol. Evol. 7(8), 990–
830 1002.
831 Thorson, J.T., Rindorf, A., Gao, J., Hanselman, D.H., Winker, H., 2016c. Density-dependent
832 changes in effective area occupied for sea-bottom-associated marine fishes. Proc. Royal
833 Soc. B. 283, 20161853. https://doi.org/10.1098/rspb.2016.1853.
834 Thorson, J.T., Barnett, L.A.K., 2017. Comparing estimates of abundance trends and distribution
835 shifts using single- and multispecies models of fishes and biogenic habitat, ICES J. of
836 Mar. Sci. 74 (5), 1311–1321. https://doi.org/10.1093/icesjms/fsw193.

837 Vidal, J., Smith, S.L., 1986. Biomass, growth, and development of populations of herbivorous
838 zooplankton in the southeastern Bering Sea during spring. Deep Sea Res. Part A.
839 Oceanographic Research Papers. 33(4), 523–556. https://doi.org/10.1016/0198-
840 0149(86)90129-9.
841 Wang, S.W., Budge, S.M., Iken, K., Gradinger, R.R., Springer, A.M., Wooller, M.J., 2015.
842 Importance of sympagic production to Bering Sea zooplankton as revealed from fatty
843 acid-carbon stable isotope analyses. Mar. Ecol. Prog. Ser. 518, 31–50.
844 https://doi.org/10.3354/meps11076.
845 Wespestad, V.G., Fritz, L.W., Ingraham, W.J., Megrey, B.A., 2000. On relationships between
846 cannibalism, climate variability, physical transport, and recruitment success of Bering
847 Sea walleye pollock (*Theragra chalcogramma*). ICES J. Mar. Sci. 57(2), 272–278.
848 Yasumiishi, E.M., Criddle, K.R., Hillgruber, N., Mueter, F.J., Helle, J. H., 2015. Chum salmon
849 (Oncorhynchus keta) growth and temperature indices as indicators of the year–class
850 strength of age-1 walleye pollock (*Gadus chalcogrammus*) in the eastern Bering Sea.
851 Fish. Oceanogr. 24(3), 242–256.
852
853

Table headings

Table 1. Pearson product moment correlation coefficient (r) for pairs of variables: copepod taxa groups: *Calanus* (C), *M. pacifica* + *Neocalanus* (MN), and C+MN from the sample-based (sb) and VAST model-based estimates; and environmental variables: sea surface temperature (SST), bottom temperature (BT), ice cover index (ICI), cold pool index (CPI) for 2002–2015 (excluding 2013). Bold indicates significant at $p < 0.05$.

Table 2. Taxa counted and identified for large copepod indices. Net mesh size is shown for stage and survey periods 2003–2011 and 2012–2016.

Table 3. Least squares linear regressions for estimates of the natural log of age-3 pollock abundance /spawning stock biomass (ln(AGE3/SSB)) as a function of SSB, sample-based (sb) and VAST modeled copepod abundance indices (C+MN, C and MN), and the cold pool index (CPI). The regression equation is: ln(Age3/SSB) = $\alpha - \beta1*SSB + \beta2*$copepod index, where α is the intercept, and $\beta1$ and $\beta2$ are coefficients of the SSB and copepod index, respectively. To more easily compare regression coefficients, the data were normalized (subtracted the mean and divided by the standard deviation of the time series), so the intercept went to zero. Statistics include t-values, R^2, corrected Akaike Information Criteria (AIC_c), and p-values.

Table 4. Stepwise backwards multiple linear regressions relating estimates of age-3 pollock abundance (AGE3) and the natural log of age-3 pollock abundance /spawning stock biomass (ln(AGE3/SSB)) to copepod indices (C+MN, C, and MN) and the cold pool index (CPI) from the pollock age-0 year. SSB was also included in regressions for estimates of ln(AGE3/SSB).

877 Statistics include R^2, AIC_c, and p-values for each variable (in order) as backward elimination
878 progressed. Bold indicates the best fit model.

879

880 Figure captions

881 Figure 1. Study area in the southeastern Bering Sea. Shelf areas are designated as Inner (< 50 m),
882 Middle (50–100 m) and Outer (100–200 m). Black dots show "knots" used in the VAST model
883 for estimates of copepod abundance. The light grey shaded region is the NOAA AFSC
884 groundfish bottom trawl survey area. The rectangle is the area used in the ice cover index.

885

886 Figure 2. Time series (2002–2016) of summer SST (ºC) and summer cold pool areal coverage
887 (km^2, divided by 10,000) in the southeastern Bering Sea in warm (red bars) and cold (blue bar)
888 years.

889

890 Figure 3. Time series of mean abundances (number m^{-2}) with standard errors for the sample-
891 based (grey line) and VAST model-based (black line) estimates of large copepods, *Calanus* spp.
892 (C), *M. pacifica* + *Neocalanus* spp. (MN), and combined estimates of C and MN (C+MN) during
893 the late summer in the southeastern Bering Sea, 2002-2016 (excluding 2013). Warm and cold
894 years designated as in Fig. 2.

895

896 Figure 4. Plots of standardized a) sample-based and b) VAST model-based estimates of
897 densities, ln([number km^{-2}] +1) of *Calanus* spp. (C) copepods in the southeastern Bering Sea,
898 2002–2016 (excluding 2013). Black dots indicate BASIS station locations.
899
900

Figure 5. Plots of standardized a) sample-based and b) VAST model-based estimates of densities, ln([number km^{-2}] +1) of *M. pacifica* + *Neocalanus* spp. (MN) copepods in the southeastern Bering Sea, 2002–2016 (excluding 2013). Black dots indicate BASIS station locations.

Figure 6. Linear least squares regressions relating age-3 pollock abundance to sample-based and VAST model-based estimates of large copepod (C+MN, C, MN) mean abundance in the southeastern Bering Sea, 2002–2015 (excluding 2013).

Figure 7. Fitted means and standard errors (red) of the age-3 pollock abundance estimated from the linear regression model using VAST model-based estimates of large copepods (C+MN) compared to pollock stock assessment estimates (black) from Ianelli et al. (2018). The predicted estimate of age-3 pollock abundance for the 2016 year class (number recruited into fishery as age-3's in 2019) is shown in blue. Pollock abundance could not be estimated from the VAST model for 2013, since copepod data were not collected that year.

Figure 8. Linear regression relating age-3 pollock abundance to the cold pool index (km^2, divided by 10,000) in the southeastern Bering Sea, 2002–2015 (excluding 2013).

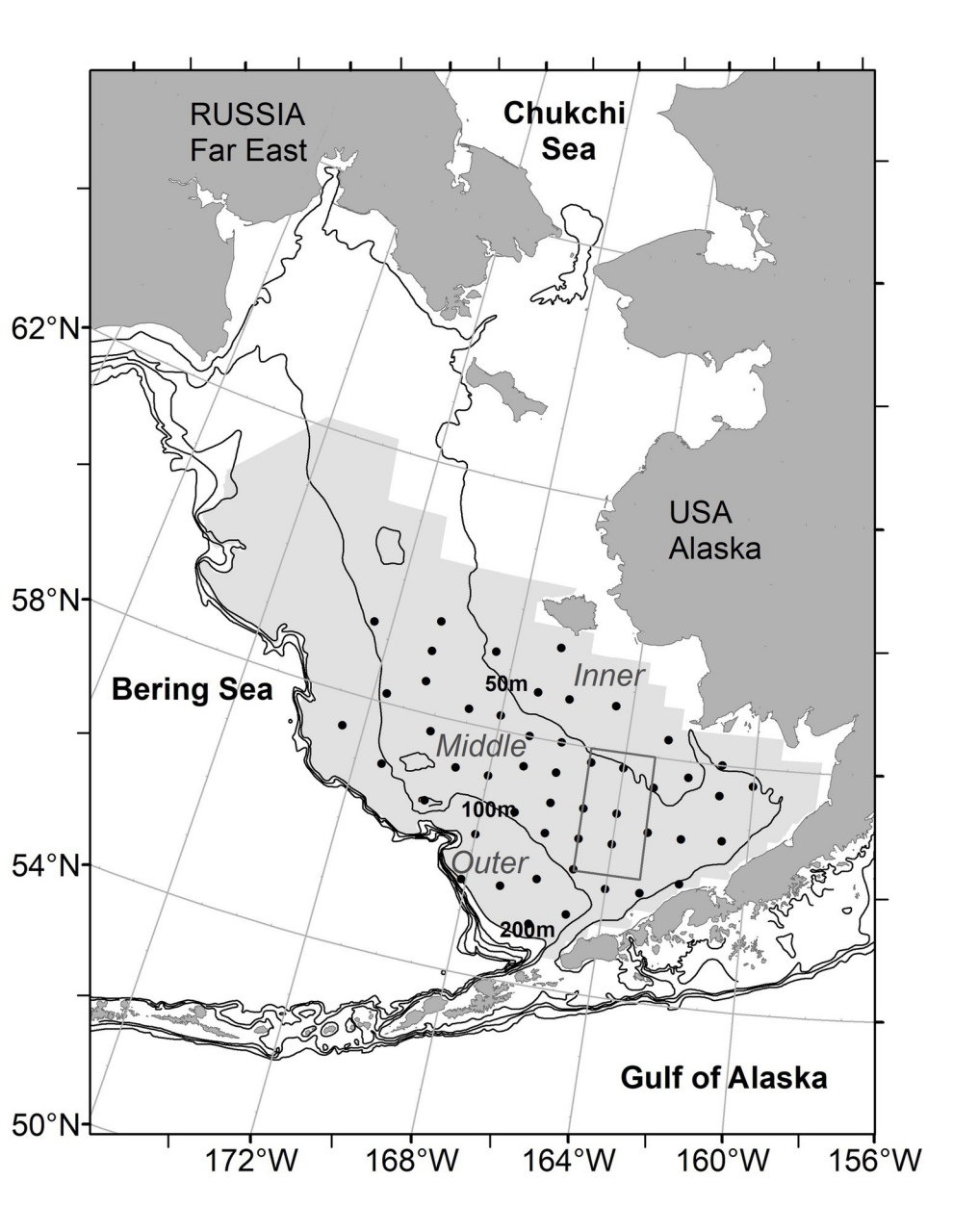
RUSSIA
Far East
Chukchi
Sea
USA
Alaska
Bering Sea
Inner
Middle
Outer
50m
100m
200m
Gulf of Alaska
62°N
58°N
54°N
50°N
172°W
168°W
164°W
160°W
156°W

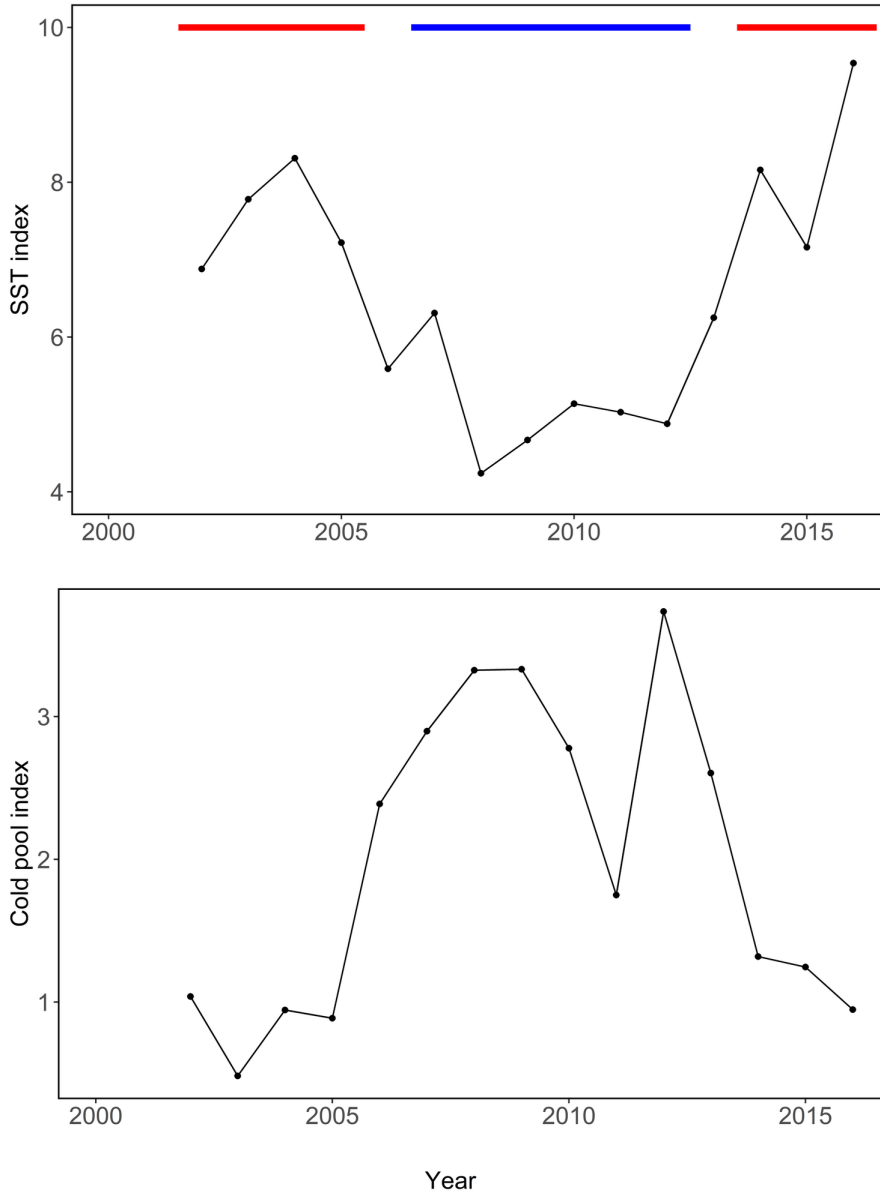
SST index
10
8
6
4
2000
2005
2010
2015
Cold pool index
3
2
1
2000
2005
2010
2015
Year

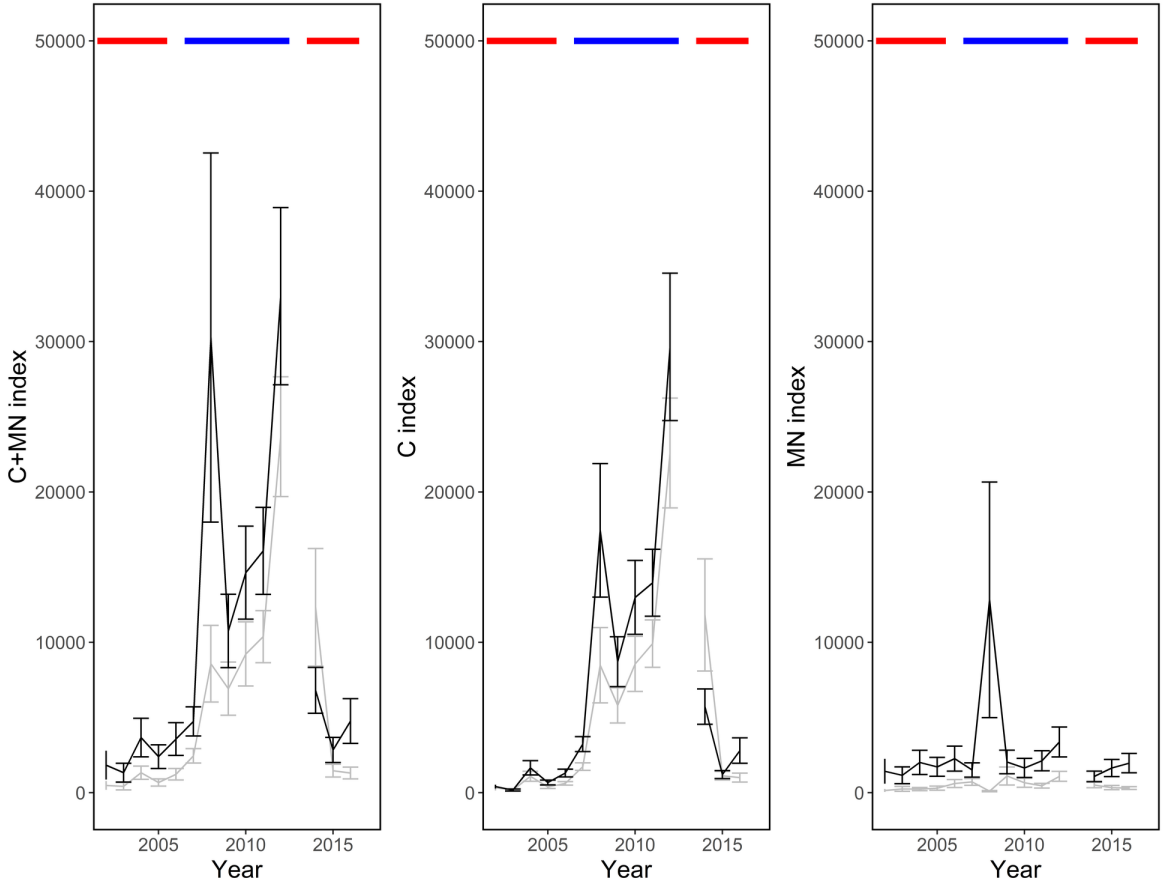
C+MN index
C index
MN index
50000
40000
30000
20000
10000
0
2005
2010
2015
Year

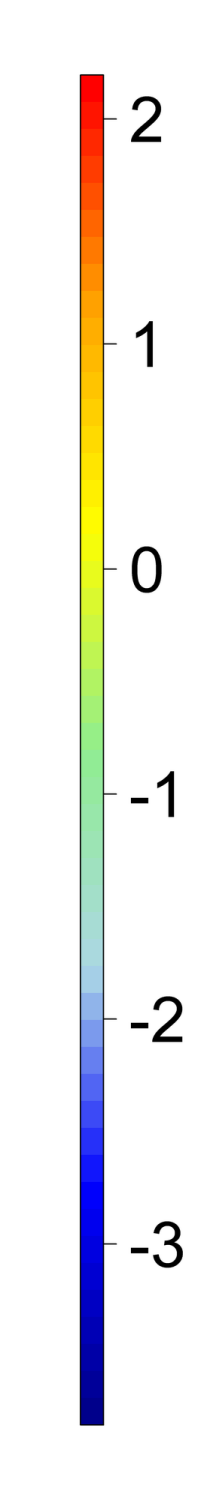
2
1
0
-1
-2
-3

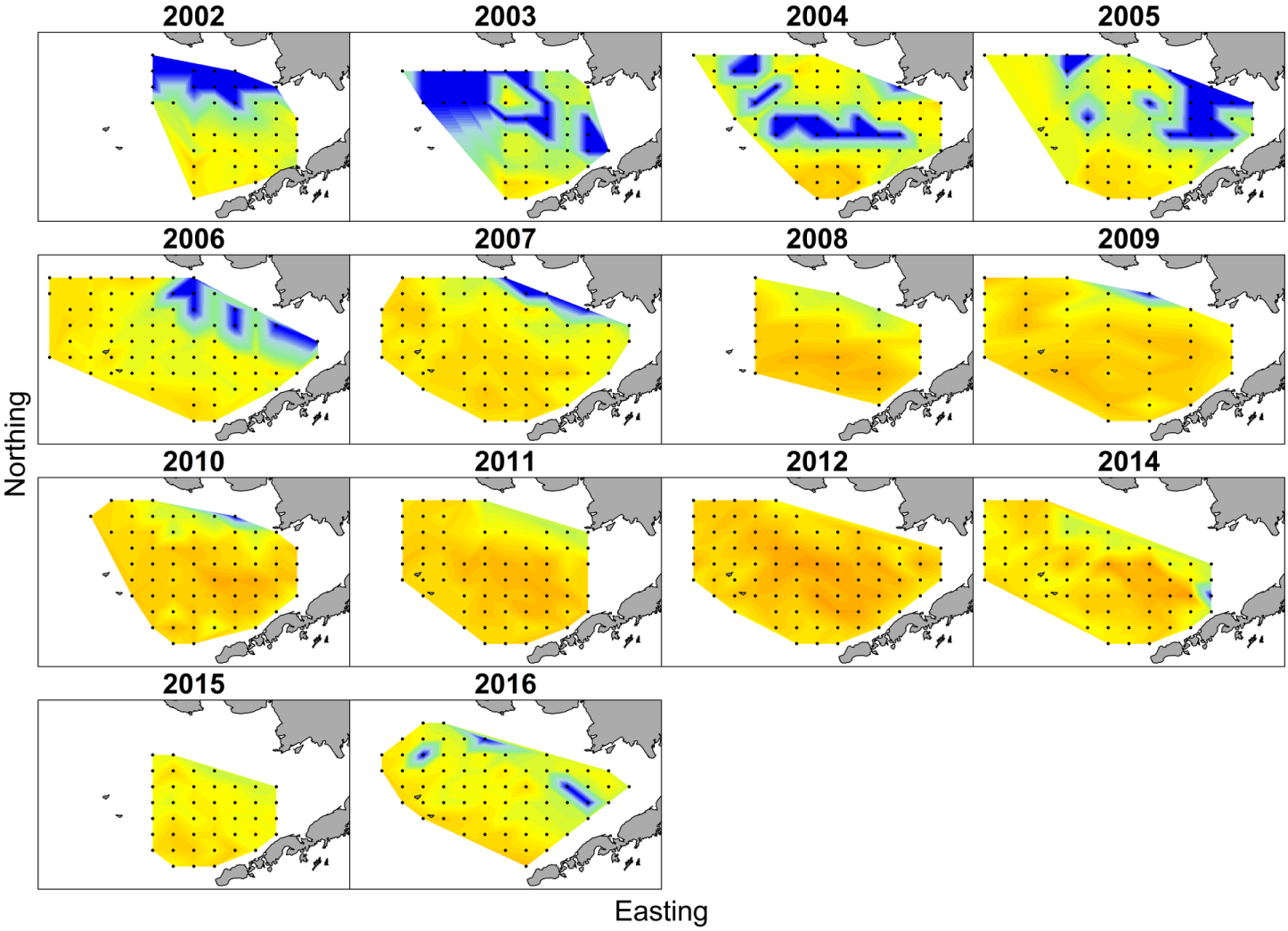
2002
2003
2004
2005
2006
2007
2008
2009
2010
2011
2012
2014
2015
2016
Northing
Easting

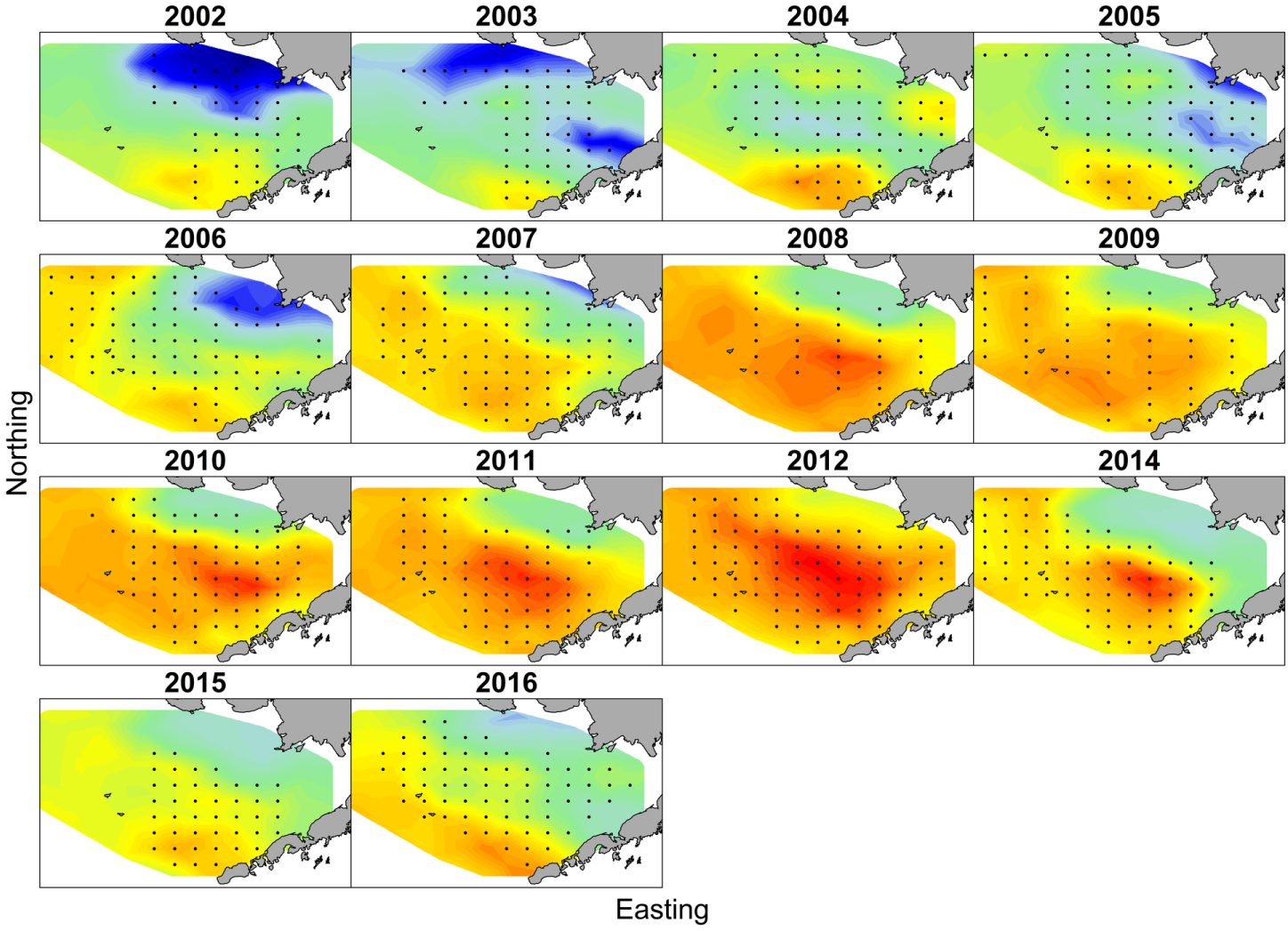
2002
2003
2004
2005
2006
2007
2008
2009
2010
2011
2012
2014
2015
2016
Northing
Easting

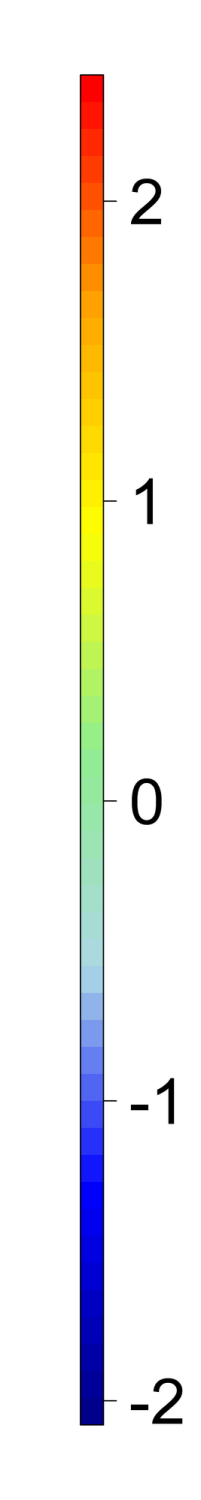
2
1
0
-1
-2

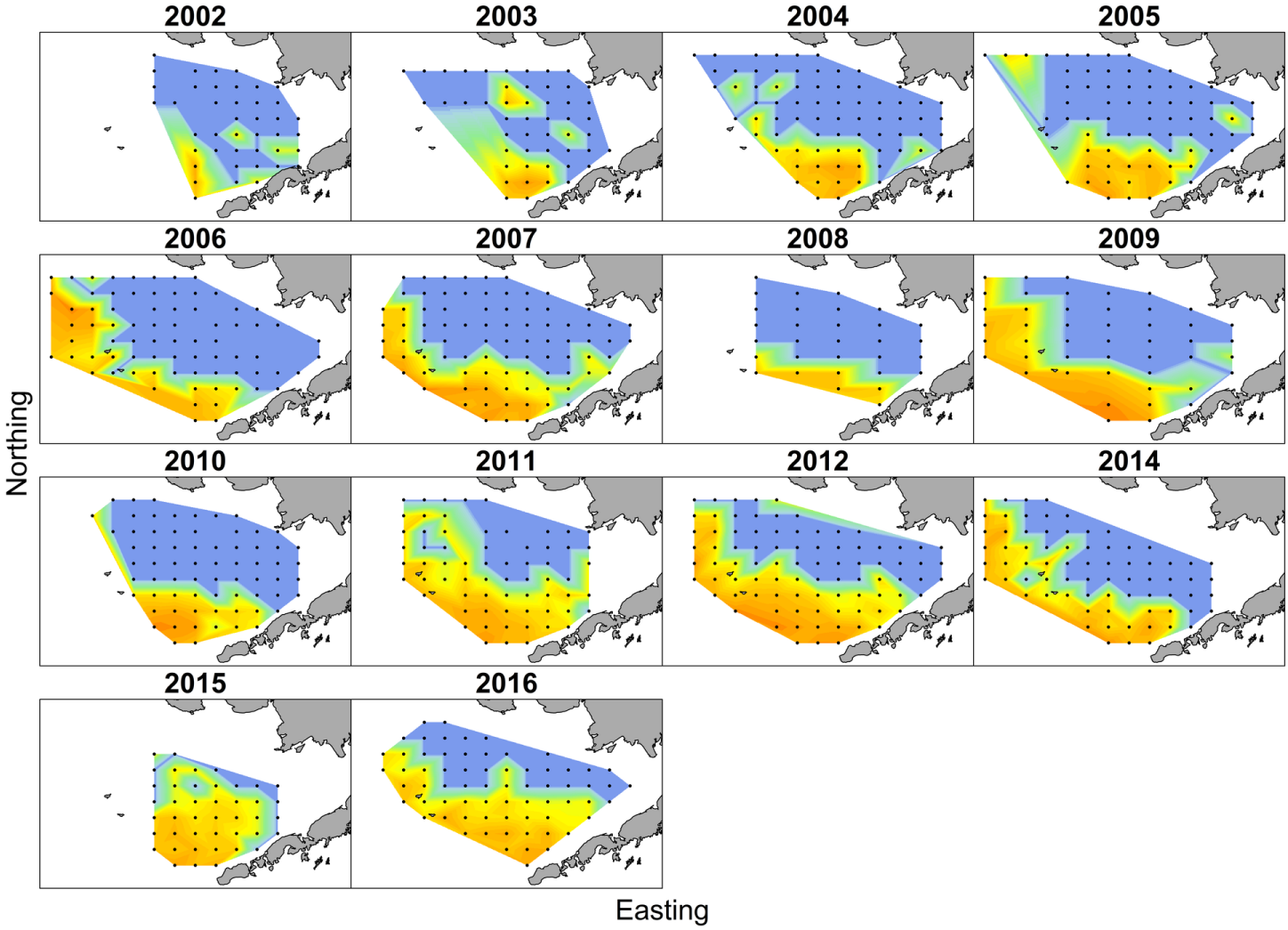
2002
2003
2004
2005
2006
2007
2008
2009
2010
2011
2012
2014
2015
2016
Northing
Easting

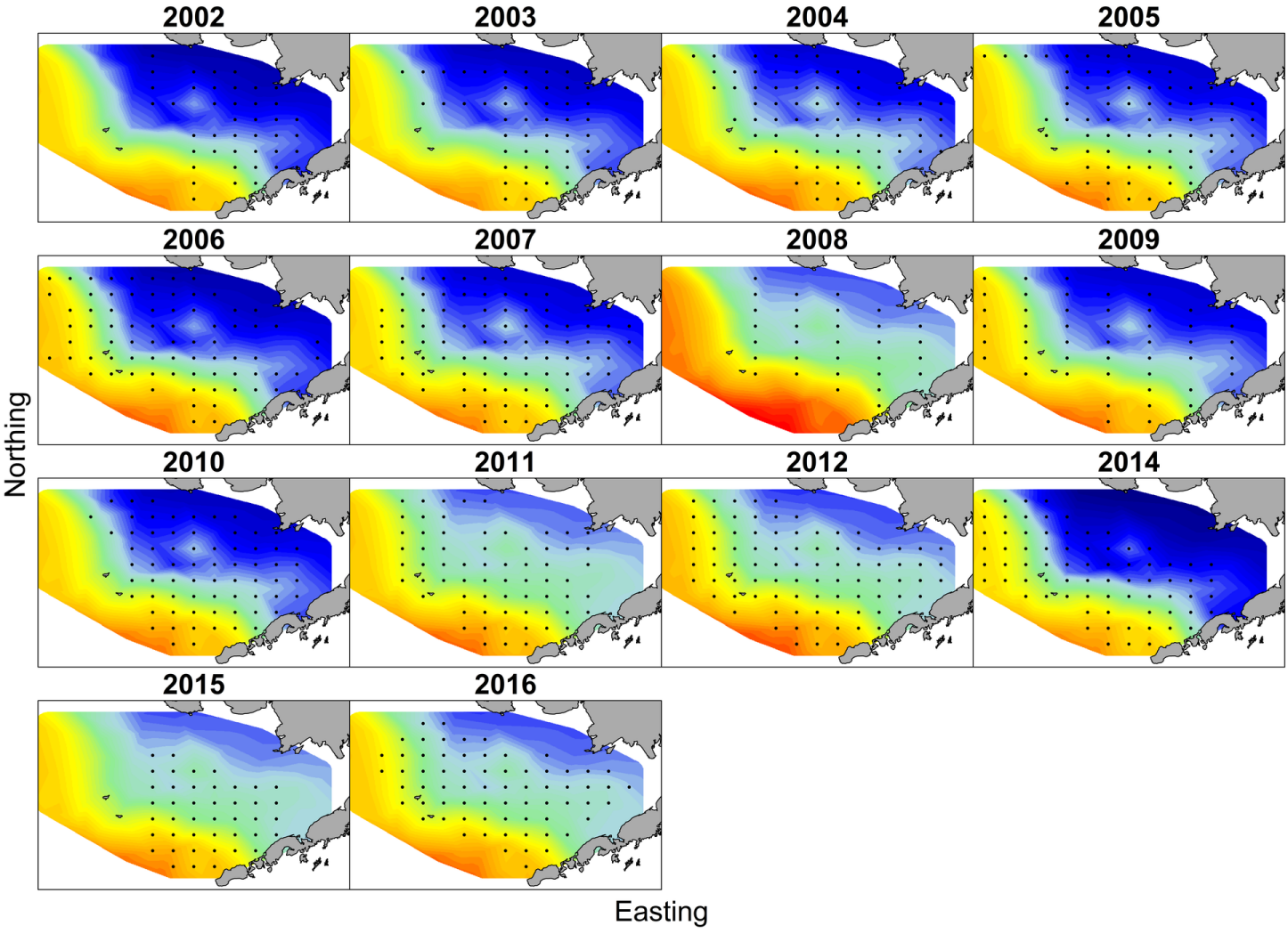
2002
2003
2004
2005
2006
2007
2008
2009
2010
2011
2012
2014
2015
2016
Northing
Easting

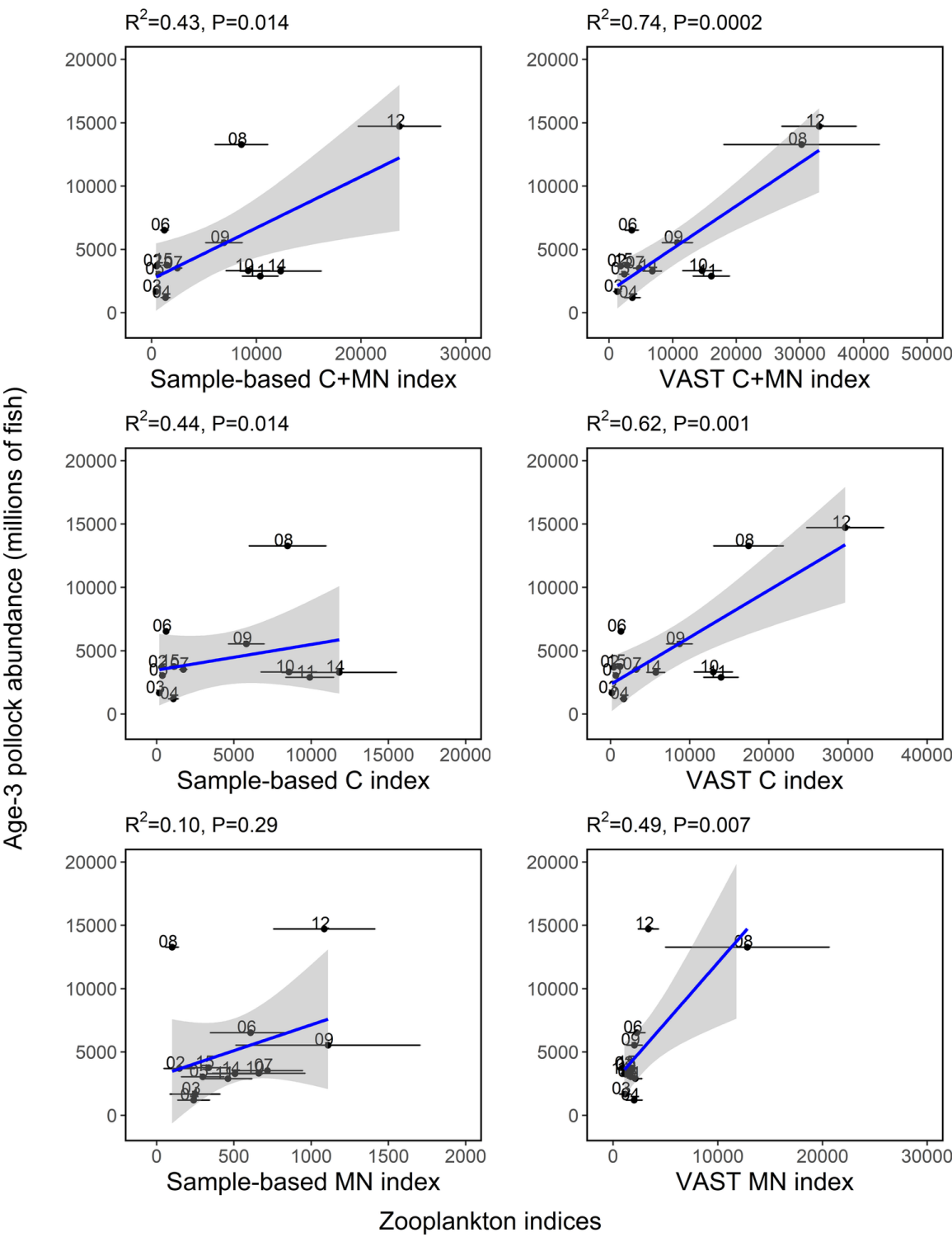
R2=0.43, P=0.014
R2=0.74, P=0.0002
Sample-based C+MN index
VAST C+MN index
R2=0.44, P=0.014
R2=0.62, P=0.001
Sample-based C index
VAST C index
R2=0.10, P=0.29
R2=0.49, P=0.007
Sample-based MN index
VAST MN index
Age-3 pollock abundance (millions of fish)
Zooplankton indices

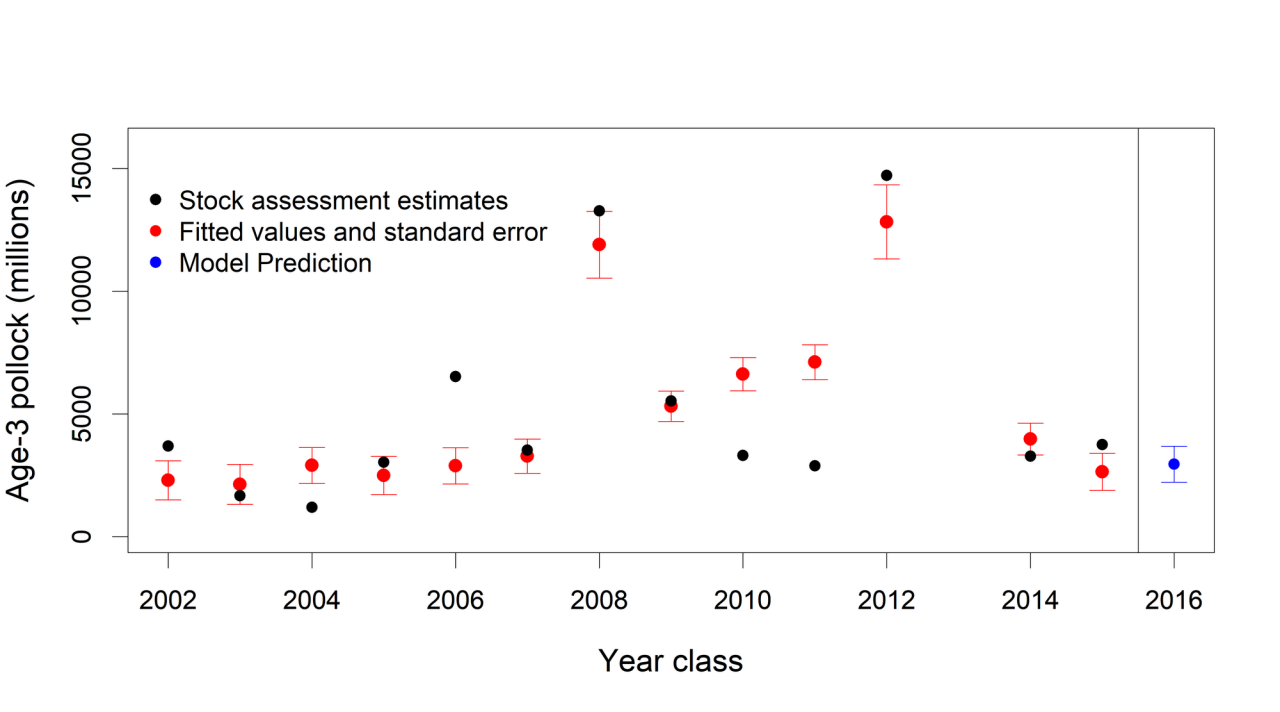
Stock assessment estimates
Fitted values and standard error
Model Prediction
Age-3 pollock (millions)
0
5000
10000
15000
2002
2004
2006
2008
2010
2012
2014
2016
Year class

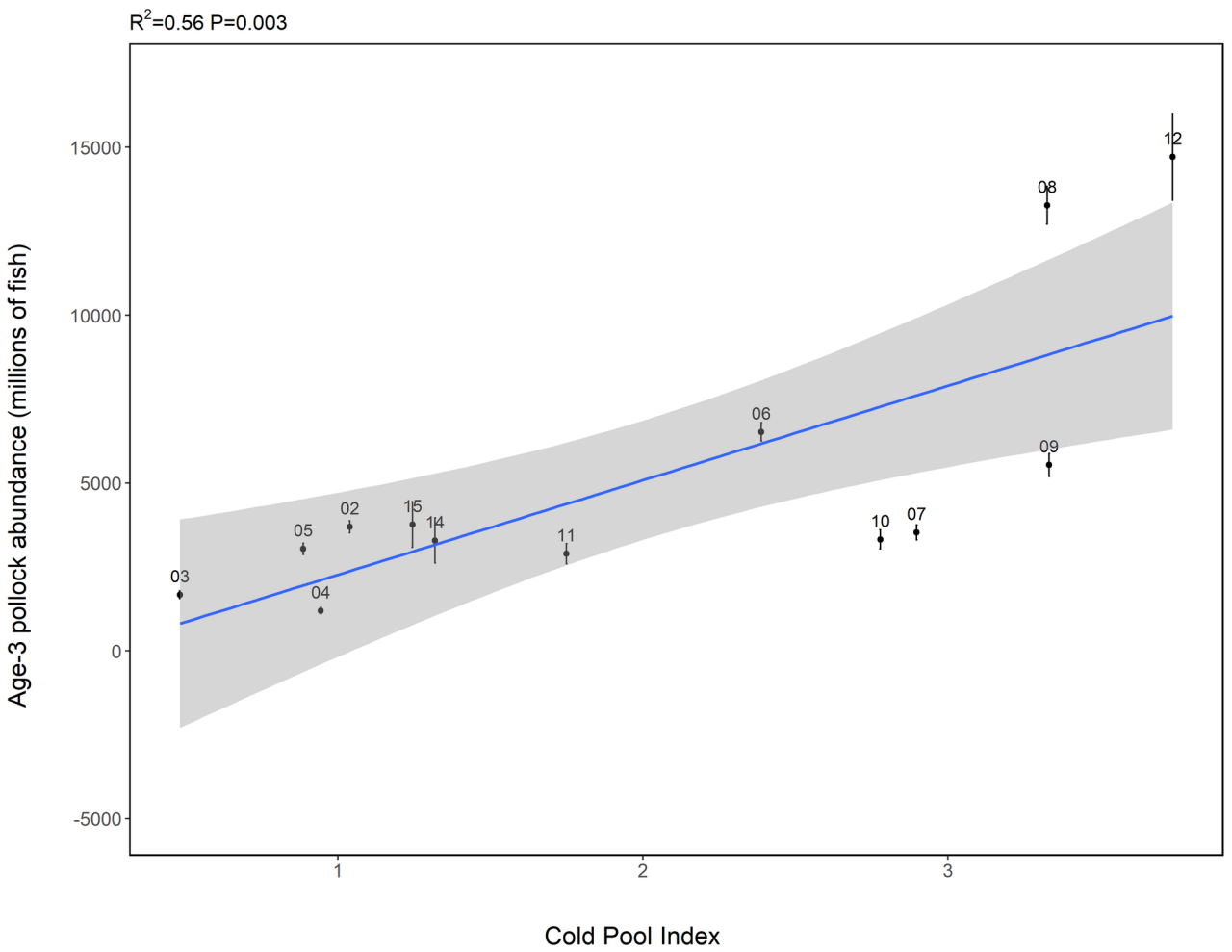
R^2=0.56 P=0.003
Age-3 pollock abundance (millions of fish)
15000
10000
5000
0
-5000
1
2
3
Cold Pool Index
03
04
05
02
15
14
11
06
10
07
08
09
12

	CMN sb	C sb	MN sb	CMN VAST	C VAST	MN VAST	SST	BT	ICI	CPI
CMN-sb	1									
C-sb	**1.00**	1								
MN-sb	**0.57**	0.54	1							
CMN-VAST	**0.83**	**0.84**	0.33	1						
C-VAST	**0.92**	**0.92**	0.49	**0.97**	1					
MN-VAST	0.22	0.24	-0.26	**0.68**	0.46	1				
SST	-0.48	-0.47	-0.47	**-0.74**	**-0.70**	-0.53	1			
BT	**-0.59**	**-0.57**	**-0.66**	**-0.74**	**-0.74**	-0.46	**0.89**	1		
ICI	**0.69**	**0.67**	**0.63**	**0.83**	**0.84**	0.44	**-0.88**	**-0.93**	1	
CPI	**0.61**	**0.59**	**0.69**	**0.75**	**0.74**	0.46	**-0.85**	**-0.99**	**0.92**	1

Taxa	Stage	Mesh size (µm) 2002-2011	Mesh size (µm) 2012-2016
Calanus marshallae/glacialis	CIII-adult	505	153
Metridia pacifica	CIV-adult	505	153
Neocalanus cristatus	CIV-adult	505	505
Neocalanus cristatus	CIII	505	153
Neocalanus flemingeri	CIII-adult	505	153
Neocalanus plumchrus	CIII-adult	505	153
Neocalanus spp.	CIII-adult	505	NA

Coeff.	Estimate	Std. Error	t -value	R^2	AIC_c	p -value
SSB	-0.75	0.20	-3.81	0.57	33.58	0.003
SSB	-0.64	0.19	-3.37	0.68	34.08	0.003
C+MN_sb	0.35	0.19	1.85			
SSB	-0.64	0.19	-3.41	0.68	34.03	0.003
C_sb	0.35	0.19	1.87			
SSB	-0.70	0.23	-3.08	0.59	37.43	0.012
MN_sb	0.14	0.23	0.62			
SSB	-0.47	0.19	-2.47	0.75	30.92	0.001
C+MN_VAST	0.51	0.19	2.67			
SSB	-0.54	0.19	-2.80	0.71	32.68	0.002
C_VAST	0.43	0.19	2.23			
SSB	-0.57	0.21	-2.77	0.67	34.56	0.004
MN_VAST	0.37	0.21	1.71			
SSB	-0.10	0.27	-0.38	0.77	29.72	0.001
CPI	0.79	0.27	2.96			

	AGE3				ln(AGE3/SSB)			
	Variables	R^2	AIC_c	p -value	Variables	R^2	AIC_c	p -value
Sample-based								
C+MN					C+MN, CPI, SSB			0.710, 0.83, 0.640
	C+MN, CPI			0.216, 0.049	CPI, SSB			0.014, 0.711
	CPI	**0.56**	**250.75**	**0.003**	**CPI**	**0.77**	**22.07**	**0**
C					C, CPI, SSB			0.663, 0.082, 0.623
	C, CPI			0.189, 0.045	CPI, SSB			0.014, 0.711
	CPI	**0.56**	**250.75**	**0.003**	**CPI**	**0.77**	**22.07**	**0**
MN					MN, CPI, SSB			0.143, 0.007, 0.874
	MN, CPI			0.185, 0.004	MN, CPI			0.114, 0.000
	CPI	**0.56**	**250.75**	**0.003**	**CPI**	**0.77**	**19.40**	**0**
VAST model								
C+MN					C+MN, CPI, SSB			0.237, 0.139, 0.568
	C+MN, CPI			0.014, 0.336	C+MN, CPI			0.248, 0.010
	C+MN	**0.74**	**243.82**	**0**	**CPI**	**0.77**	**22.07**	**0**
C					C, CPI, SSB			0.543, 0.128, 0.596
	C, CPI			0.076, 0.203	C, CPI			0.627, 0.005
	C	**0.62**	**248.66**	**0.001**	**CPI**	**0.77**	**22.07**	**0**
MN					MN, CPI, SSB			0.059, 0.009, 0.882
	MN, CPI	**0.72**	**249.14**	**0.037, 0.017**	**MN, CPI**	**0.85**	**20.83**	**0.043, 0.000**